



**HAL**  
open science

## Molecular mechanisms of mutualistic and antagonistic interactions in a plant-pollinator association

Rong Wang, Yang Yang, Yi Jing, Simon T. Segar, Yu Zhang, Gang Wang, Jin Chen, Qing-Feng Liu, Shan Chen, Yan Chen, et al.

► **To cite this version:**

Rong Wang, Yang Yang, Yi Jing, Simon T. Segar, Yu Zhang, et al.. Molecular mechanisms of mutualistic and antagonistic interactions in a plant-pollinator association. *Nature Ecology & Evolution*, 2021, 5 (7), pp.974-986. 10.1038/s41559-021-01469-1 . hal-03231509

**HAL Id: hal-03231509**

**<https://hal.inrae.fr/hal-03231509>**

Submitted on 9 Nov 2021

**HAL** is a multi-disciplinary open access archive for the deposit and dissemination of scientific research documents, whether they are published or not. The documents may come from teaching and research institutions in France or abroad, or from public or private research centers.

L'archive ouverte pluridisciplinaire **HAL**, est destinée au dépôt et à la diffusion de documents scientifiques de niveau recherche, publiés ou non, émanant des établissements d'enseignement et de recherche français ou étrangers, des laboratoires publics ou privés.

1 doi: 10.1038/s41559-021-01469-1

2 Nat Ecol Evol 5, 974–986 (2021).

3 Molecular mechanisms of mutualistic and antagonistic interactions in a  
4 plant-pollinator association

5 Rong Wang<sup>1,20†</sup>, Yang Yang<sup>1†</sup>, Yi Jing<sup>2†</sup>, Simon T. Segar<sup>3†</sup>, Yu Zhang<sup>1</sup>, Gang Wang<sup>4</sup>,

6 Jin Chen<sup>4</sup>, Qing-Feng Liu<sup>2</sup>, Shan Chen<sup>1</sup>, Yan Chen<sup>5</sup>, Astrid Cruaud<sup>6</sup>, Yuan-Yuan

7 Ding<sup>1</sup>, Derek Dunn<sup>7</sup>, Qiang Gao<sup>2</sup>, Philip M. Gilmartin<sup>8,9</sup>, Kai Jiang<sup>1</sup>, Finn Kjellberg<sup>10</sup>,

8 Hong-Qing Li<sup>11</sup>, Yuan-Yuan Li<sup>1</sup>, Jian-Quan Liu<sup>12</sup>, Min Liu<sup>13</sup>, Carlos A. Machado<sup>14</sup>,

9 Ray Ming<sup>15</sup>, Jean-Yves Rasplus<sup>6</sup>, Xin Tong<sup>1</sup>, Ping Wen<sup>4</sup>, Huan-Ming Yang<sup>2</sup>, Jing-Jun

10 Yang<sup>1</sup>, Ye Yin<sup>2</sup>, Xing-Tan Zhang<sup>16</sup>, Yuan-Ye Zhang<sup>17</sup>, Hui Yu<sup>18,19\*</sup>, Zhen Yue<sup>2\*</sup>,

11 Stephen G. Compton<sup>9\*</sup>, Xiao-Yong Chen<sup>1,20\*</sup>

12

13 <sup>1</sup> Zhejiang Tiantong Forest Ecosystem National Observation and Research Station,

14 School of Ecological and Environmental Sciences, East China Normal University,

15 Shanghai 200241, China

16 <sup>2</sup>BGI Genomics, BGI-Shenzhen, Shenzhen 518083, China

17 <sup>3</sup>Agriculture & Environment Department, Harper Adams University, Newport, TF10

18 8NB, United Kingdom

19 <sup>4</sup>CAS Key Laboratory of Tropical Forest Ecology, Xishuangbanna Tropical Botanical

20 Garden, Chinese Academy of Sciences, Mengla, Yunnan Province 666303, China

21 <sup>5</sup>Ecological Security and Protection Key Laboratory of Sichuan Province, Mianyang

22 Normal University, Mianyang 621000, China

23 <sup>6</sup>INRA, UMR1062 CBGP, F-34988 Montferrier-sur-Lez, France

24 <sup>7</sup>College of Life Sciences, Northwest University, Xi'an, Shaanxi 710069, China

25 <sup>8</sup> School of Biology, University of Hull, Hull HU6 7RX, UK

26 <sup>9</sup>School of Biology, University of Leeds, Leeds LS2 9JT, UK

27 <sup>10</sup>CEFE, CNRS, Univ Montpellier, Univ Paul Valéry Montpellier, EPHE, IRD, France

28 <sup>11</sup>School of Life Sciences, East China Normal University, Shanghai 200241, China

29 <sup>12</sup>Key Laboratory of Bio-resource and Eco-environment of Ministry of Education,  
30 College of Life Sciences, Sichuan University, Chengdu 610065, China.

31 <sup>13</sup>School of Life Sciences, Guangzhou University, Guangzhou 510006, China

32 <sup>14</sup>Department of Biology, University of Maryland, College Park, MD 20742, The  
33 United States of America

34 <sup>15</sup>FAFU and UIUC-SIB Joint Center for Genomics and Biotechnology, Fujian  
35 Agriculture and Forestry University, Fuzhou 350002, China; Department of Plant  
36 Biology, University of Illinois at Urbana-Champaign, Urbana, IL 61801, USA.

37 <sup>16</sup>Center for Genomics and Biotechnology, Fujian Provincial Key Laboratory of  
38 Haixia Applied Plant Systems Biology, Key Laboratory of Genetics, Breeding and  
39 Multiple Utilization of Corps, Ministry of Education, Fujian Agriculture and  
40 Forestry University, Fuzhou 350002, China.

41 <sup>17</sup>Key Laboratory of the Ministry of Education for Coastal and Wetland Ecosystems,  
42 College of the Environment and Ecology, Xiamen University, Xiamen, Fujian  
43 361102, China

44 <sup>18</sup>Key Laboratory of Plant Resource Conservation and Sustainable Utilization, South

45 China Botanical Garden, Chinese Academy of Sciences, Guangzhou 510650,

46 China

47 <sup>19</sup>School of Life Sciences, Qufu Normal University, Qufu Shandong, 273165, China

48 <sup>20</sup>Shanghai Institute of Pollution Control and Ecological Security, Shanghai 200092,

49 China

50

51 † These authors contributed equally to this work.

52 \* Co-corresponding authors.

53 E-mail: xychen@des.ecnu.edu.cn (X.-Y.C.); yuhui@scib.ac.cn (H.Y.);

54 S.G.A.Compton@leeds.ac.uk (S.G.C.); yuezhen@bgi.com (Z.Y.)

55

56 **Abstract**

57 Many insects metamorphose from antagonistic larvae into mutualistic adult  
58 pollinators, with reciprocal adaptation leading to specialized insect-plant associations.  
59 It remains unknown how such interactions are established at molecular level. Here we  
60 assembled high-quality genomes of a fig species, *Ficus pumila* var. *pumila*, and its  
61 specific pollinating wasp, *Wiebesia pumilae*. We combined multi-omics with  
62 validation experiments to reveal molecular mechanisms underlying this specialized  
63 interaction. In the plant, we identified the specific compound attracting pollinators and  
64 validated the function of several key genes regulating its biosynthesis. In the  
65 pollinator, we found a highly reduced number of odorant-binding protein (OBP) genes  
66 and an OBP mainly binding the attractant. During antagonistic interaction, we found  
67 similar chemical profiles and turnovers throughout the development of galled ovules  
68 and seeds, and a significant contraction of detoxification-related gene families in the  
69 pollinator. Our study detects some key genes bridging coevolved mutualists,  
70 establishing expectations for more diffuse insect-pollinator systems.

71

72 **Keywords**

73 Multi-omics, plant-pollinator mutualism, insect-host identification, pollinator  
74 adaptation to host plant, gene for gene coadaptation

75

76 **Introduction**

77 Evolutionary adaptation fuels the genetic diversification of living organisms,  
78 driving speciation and emergent biodiversity<sup>1,2</sup>. However, in contrast to adaptation to  
79 abiotic conditions<sup>3-5</sup>, it remains unclear how species adapt to reciprocally evolving  
80 biotic factors at the molecular level. This reflects the difficulty of identifying the traits  
81 linking interspecific interactions in a dynamic selective landscape. The high diversity  
82 of phytophagous insects and angiosperms is believed to be the result of coevolution,  
83 in part driven by ongoing insect-plant arms races<sup>6,7</sup>. Many herbivorous insects are also  
84 responsible for mediating gene flow between plant populations, often occurring as  
85 both antagonistic (i.e., herbivorous) larvae and mutualistic pollinating adults<sup>8</sup>.  
86 Selection by multiple agents associated with herbivorous/pollinating insects acts on  
87 floral traits to both deter herbivores and attract pollinators<sup>9</sup>, making it difficult to  
88 separate mechanistic processes in many plant-pollinator systems. Tightly co-evolved  
89 species often have more apparent interacting traits, which provide an excellent testing  
90 ground for exploring coadaptation.

91 The obligate mutualisms comprising ~800 species from the genus *Ficus*  
92 (Moraceae) and their host specific pollinating wasps (fig wasps; Hymenoptera,  
93 Agaonidae) form a classical example of coevolution and contribute greatly to  
94 ecosystem functioning, biodiversity and agriculture<sup>10,11</sup>. Both mutualists have evolved  
95 strict correspondence in morphological, metabolic and life history traits<sup>10,12</sup>. The  
96 plants reward the larvae of pollinating wasps with nutrition and protection, and each  
97 mutualist wasp species is both pollinator and herbivore<sup>12</sup>. Each individual wasp

98 spends the majority of its lifespan at the larval stage (from three weeks up to nine  
99 months) and develops inside a single galled ovule of a female floret located inside the  
100 enclosed inflorescences characteristic of the genus (figs or ‘syconia’)<sup>13-15</sup> (Fig. 1a).  
101 There are two predominant types of breeding systems in *Ficus* species, monoecy and  
102 dioecy<sup>16</sup>. In monoecious figs, each fig produces female florets that can be either  
103 pollinated or galled by pollinator larvae. In dioecious species, only the female florets  
104 (feeder florets) in figs of functional male trees support the development of pollinator  
105 offspring; figs growing on female trees attract pollinators to fertilize the female florets  
106 (seed florets) that do not support wasp development (Fig. 1a). Upon locating host figs,  
107 adult female wasps must crawl through a narrow passage usually lined by bracts (the  
108 ostiole), into a dark central lumen where they typically remain trapped following  
109 oviposition and/or pollination. Short lived (usually shorter than three days) adult  
110 wasps do not feed<sup>10</sup>.

111 Central to mediating these species-specific interactions are plant-emitted volatile  
112 organic compounds (VOCs), which guide adult female wasps to precisely identify and  
113 locate host figs<sup>13,14,17-21</sup>. Moreover, the high-quality genomes of a *Ficus* species and its  
114 pollinating wasp (*Ficus microcarpa* and *Eupristina verticillata*) have been recently  
115 reported<sup>11</sup>, which create a basis for exploring how these pollinators identify host figs  
116 at the molecular level. However, to date the key attractive VOCs have only been  
117 explicitly identified in a small number of fig-pollinator mutualisms<sup>17,18</sup>, and the  
118 underlying molecular mechanisms determining host-specific signaling and insect  
119 attraction remain unknown.

120       Once the problem of host identification has been overcome, pollinator larvae  
121 must also survive and develop under a set of unique conditions inside galled ovules  
122 that support their development (Fig. 1a). While figs can defend against herbivores  
123 from a wide range of taxa<sup>22</sup>, it is unclear how pollinator larvae cope with plant  
124 defensive chemicals inside the galled ovules during this antagonistic phase of  
125 mutualism. One possible explanation is that galling behavior may activate the plant  
126 reproductive program in galled tissues, so that galling insects can avoid the strong  
127 chemical defenses induced by stress reaction when they utilize plant nutrients<sup>23-25</sup>. To  
128 test whether the reproductive program is activated in galled ovules, it is necessary to  
129 compare between the chemical profiles of galled ovules and seeds. We also expect  
130 that such adaptation to a specialized environment must leave molecular footprints in  
131 pollinator genome, for example contracted detoxification-related gene families<sup>26,27</sup>.

132       Here we focused on a fig-pollinator mutualism comprising a dioecious *Ficus*  
133 species *Ficus pumila* var. *pumila*<sup>28</sup> and its specific pollinator *Wiebesia pumilae*<sup>29</sup> (Fig.  
134 1a). We used multi-omics in combination with validation experiments to unravel the  
135 key molecular mechanisms contributing to the antagonistic and the mutualistic  
136 interactions in this system. We determined the specific attractive VOC and several key  
137 genes relevant to its biosynthesis. We identified the corresponding responses in the  
138 odorant-binding protein (OBP) genes in the pollinator genome and an OBP mainly  
139 binding the attractant. During the antagonistic phase, we found a similar turnover of  
140 secondary metabolites when female florets developed into either galled ovules or  
141 seeds, and almost identical chemical profiles between these two tissues. It implies that

142 the galled ovules may develop like seeds. A contraction of detoxification-related gene  
143 families was found in the pollinator genome, providing insights into the fig-pollinator  
144 coadaptation during antagonistic interaction.

## 145 **Results**

### 146 **Assembly of genomes and evolution**

147 To provide high-quality reference genomes for transcriptomic and proteomic  
148 analyses, we assembled genomes of *F. pumila* var. *pumila* and *W. pumilae* using a  
149 combination of Illumina and PacBio sequencing technologies (Supplementary Table  
150 1; see Methods). The assembled genomes were 315.7 Mb (contig N50 of 2.3 Mb) for  
151 the plant and 318.2 Mb (contig N50 of 10.9 Mb) for the pollinator (Table 1 and  
152 Supplementary Table 2). Using the uniquely mapped reads produced by the high-  
153 throughput chromatin conformation capture (Hi-C) technique (Supplementary Tables  
154 1, 2), we generated Hi-C-based physical maps composed of 13 and 6 pseudo-  
155 chromosomes, with 96.6% (305 Mb) and 99.8% (318 Mb) of the assembled genomes  
156 anchored to the pseudo-chromosomes (Table 1 and Supplementary Fig. 1). The  
157 scaffold N50 of the assembled genomes were 22.4 Mb and 59.4 Mb, and the pseudo-  
158 chromosomes included 97.1% (27,378) and 99.8% (12,292) of protein-coding genes  
159 (Table 1). Genome annotation results showed that the structures and functions of  
160 25,905 and 12,305 protein-coding genes were annotated in the two genomes  
161 (Supplementary Figs. 2 and Supplementary Tables 3-5). BUSCO quality analysis of  
162 annotation showed that 92.4% of 1375 conserved plant genes and 91.3% of 4,415  
163 Hymenoptera genes have complete coverage (Supplementary Table 3).

164 The protein-coding genes of *F. pumila* var. *pumila* and *W. pumilae* were clustered  
165 into 15,631 and 7,969 gene families (Supplementary Fig. 3 and Supplementary Table  
166 6). Analysis of comparative genomics using the genomes of 13 Angiosperm species  
167 including *F. pumila* var. *pumila* and three congeneric species (*Ficus hispida*<sup>11</sup>, *Ficus*  
168 *microcarpa*<sup>11</sup> and *Ficus carica*<sup>16</sup>) showed that in the common ancestors of the four  
169 *Ficus* species, 1,473 gene families had contracted and 888 gene families had  
170 expanded. Phylogenetic reconstruction revealed that *F. hispida* is more closely related  
171 to *F. pumila* var. *pumila* than the other two *Ficus* species (Supplementary Fig. 4a). In  
172 the analysis of comparative genomics using the genomes of 11 arthropod species  
173 containing *W. pumilae* and two other pollinator wasp species (*Ceratosolen solmsi*<sup>11</sup>  
174 and *Eupristina verticillata*<sup>27</sup>), we found 48 expanded and 1261 contracted gene  
175 families in the common ancestors of three pollinating wasp species. We recovered a  
176 group containing and *E. verticillata* and *W. pumilae* with *C. solmsi* as its sibling  
177 (Supplementary Fig. 4b). There was no evidence for recent whole-genome duplication  
178 in the plant, and only a few small segments (total length of 1.3 Mb) were found to be  
179 duplicated in the pollinator genome (Supplementary Fig. 5).

#### 180 **Attractive compound forming fig-pollinator identification**

181 At the receptive stage, figs release VOCs containing critical compound(s)  
182 attracting their pollinating wasps (Fig. 1a). To determine the attractive compound(s),  
183 we collected VOCs from functional male and female figs of *F. pumila* var. *pumila* at  
184 the pre-repetitive and the receptive stages using the dynamic headspace sampling  
185 (DHS) approach, and identified a total of 70 compounds (Fig. 1a and Supplementary

186 Tables 7, 8). Only three (linalool, nonanal and decanal) of these compounds were  
187 found to elicit physiological responses of adult females of *W. pumilae* (Fig. 1b, c), of  
188 which only decanal was emitted exclusively at the receptive stage (Supplementary  
189 Table 8). We then conducted behavioral preference tests among the three compounds  
190 using 50 female pollinating wasps in each testing group. The wasps showed a  
191 significantly greater preference for decanal than the control and a significantly  
192 reduced preference for nonanal than the control, with a similar preference between  
193 decanal and a nonanal-decanal blend (Fig. 1d and Supplementary Table 9). These  
194 results demonstrate that the VOC compound decanal, emitted by *F. pumila* var. *pumila*  
195 figs at the receptive stage, functions to attract the pollinating wasp *W. pumilae*.

196

### 197 **Molecular mechanisms of specific host identification**

198 To identify the molecular mechanisms underlying the behavioral responses of *W.*  
199 *pumilae* to the VOCs emitted by its host figs, we annotated the four gene families  
200 involved in insect olfaction<sup>30</sup>. Across these gene families, *W. pumilae*, *E. verticillata*  
201 and *C. solmsi* consistently have lower numbers of genes, and, in particular, the  
202 number of odorant-binding protein (OBP) genes is significantly lower than less host-  
203 specific insects (Fig. 2a). Phylogenetic and synteny analysis including genomes of the  
204 three pollinating wasp species and the distantly related *Nasonia vitripennis* showed  
205 that most OBP genes in the pollinating wasp species displayed strong homology and  
206 that the small number of OBP genes resulted from gene loss and infrequent tandem  
207 duplication (Supplementary Figs. 6a, 7a). There were apparent differences in motif

208 structure among OBPs in six of the ten syntenic blocks (Supplementary Fig. 6b). The  
209 general contraction in OBP genes and frequent changes in motif structure of  
210 homologous OBPs among pollinating wasp species may be expected given their high  
211 host specificity and different VOC cues used for detecting host figs.

212 Among the 12 OBP genes of *W. pumilae*, transcriptome and proteome evidence  
213 showed that all genes were transcribed but only seven are translated into detectable  
214 proteins in adult females (Fig. 2b, Supplementary Fig. 8 and Supplementary Table 7).  
215 There were no proteins with significant differences in quantity (PSDs) and  
216 differentially expressed genes (DEGs) between the control and the VOCs-contacting  
217 treatment (Supplementary Table 10).

218 To explore functions of *W. pumilae* OBPs, we predicted motif structures of OBPs  
219 and compared them with the OBPs in *Adelphocoris lineolatus*<sup>31</sup> and *Culex*  
220 *quinquefasciatus*<sup>32</sup>, known to have decanal or nonanal binding activity. Among the  
221 seven OBPs with detectable protein products, WpumOBP2 shows similar structure to  
222 the known decanal-binding protein and WpumOBP11 is similar to the known  
223 nonanal-binding protein (Fig. 2c and Supplementary Fig. 9). To validate the functions  
224 of WpumOBP2 and WpumOBP11, we produced the recombinant proteins for these  
225 two OBPs and measured their binding affinity to decanal and nonanal using surface  
226 plasmon resonance (SPR) experiments. Consistent with the prediction, the  
227 experiments revealed considerably lower  $K_D$  (representing much higher binding  
228 affinity) of WpumOPB2 to decanal than to nonanal and far lower  $K_D$  of WpumOBP11  
229 to nonanal than to decanal, and thus demonstrate the high binding affinity of these two

230 OBPs to the corresponding compounds (Fig 2d, Supplementary Fig. 10 and  
231 Supplementary Table 11). Therefore, these results provide solid evidence that  
232 WpumOBP2 is the main binding protein to the attractant, and pollination of *F. pumila*  
233 *var. pumila* by *W. pumilae* is initiated by the binding of decanal with WpumOPB2.

234

### 235 **Regulation of gene expression in attractant biosynthesis**

236 To identify the tissue for attractant emission within figs, we measured the  
237 concentration of decanal emitted by ostiolar tissues and female florets at the receptive  
238 stage from both sexes of *F. pumila var. pumila* (Fig. 1a) using DHS, as previous  
239 studies from other species suggested VOCs are mainly released from these tissues<sup>13,20</sup>.  
240 The concentration of collected decanal in ostiolar tissues was  $3.13 \pm 1.11$  pg/g, which  
241 was 9.1 times as that in female florets ( $0.34 \pm 0.05$  pg/g) (Pairwise T Test: df=9,  
242  $t=6.02$ ,  $p=0.002$ ). Thus, the results revealed that decanal was predominantly emitted  
243 by ostiolar tissues at a similar concentration between sexes (T Test: df=4,  $t=0.20$ ,  
244  $p=0.858$  in ostiolar tissues; df=4,  $t=0.24$ ,  $p=0.826$  in female florets).

245 To identify key genes involved in the biosynthesis of decanal, we conducted  
246 transcriptome and proteome analysis on ostiolar tissues collected at the pre-receptive  
247 and the receptive stages (Supplementary Table 7). The biosynthesis of decanal and  
248 nonanal is involved in the pathways of fatty acid biosynthesis (ko00061), elongation  
249 (ko00062) and metabolism (ko00071 and ko00592) (Fig. 3a)<sup>33,34</sup>. Genes in these  
250 pathways showed similar patterns of expression between transcriptome and proteome  
251 data (Supplementary Fig. 11 and Supplementary Table 12). Comparing the receptive

252 with the pre-receptive stage, we detected a total of eight PSDs (Fig. 3b), likely  
253 facilitating the biosynthesis of decanal and suppressing the biosynthesis of nonanal at  
254 the receptive stage (Fig. 3a). Down-regulated PSDs included two ACSLs (long-chain  
255 acyl-CoA synthetase) and one HACD (very-long-chain (3R)-3-hydroxyacyl-CoA  
256 dehydratase), while up-regulated PSDs comprised an ALDH (acetaldehyde  
257 dehydrogenase), an ADH (alcohol dehydrogenase), two LOX2Ss (lipoxygenase) and  
258 one HPL (hydroperoxide lyase) (Fig. 3b). To validate the function of key genes (the  
259 two ACSLs, the ALDH and the ADH) in decanal biosynthesis, we produced the  
260 recombinant proteins of these genes and conducted *in vitro* enzyme activity assay (see  
261 Methods). The final products of the *in vitro* reactions identified by LC-MS or GC-  
262 MS are consistent with the standards (Fig. 3 c-e). These results validate the enzyme  
263 activity of the two ACSLs in synthesizing hexadecanoyl-CoA as well as the ALDH  
264 and the ADH in synthesizing decanal and decanol.

265 To understand the transcriptional regulation of decanal biosynthesis, we  
266 conducted co-expression network analysis and found one module containing two key  
267 genes (*FpumACSL10* and *FpumALDH1*) and four potential regulating transcription  
268 factors (two *HD-ZIPs*, one *bHLH* and one *bZIP*) (Fig. 3f and Supplementary Table  
269 13). Cis-element detection analysis revealed one G-box motif upstream of  
270 *FpumACSL10* and six G-box and one HD-Zip motifs upstream of *FpumALDH1*  
271 (Supplementary Table 14). As G-box binds to transcription factor families of bZIPs  
272 and bHLHs and HD-Zip binds to HD-ZIPs<sup>35,36</sup>, we hypothesized that expression of  
273 *FpumACSL10* is regulated by the bHLH and the bZIP and all above four transcription

274 factors regulate the expression of *FpumALDH1*. To test this hypothesis, we obtained  
275 qualified polyclonal antibodies for the four transcription factors and performed ChIP-  
276 qPCR experiments. High % input and fold enrichment values showed that the bHLH  
277 and the bZIP could bind to the promoter region of *FpumACSL10* and all the four  
278 transcription factors could bind to the promoter region of *FpumALDH1* (Fig. 3g, h),  
279 providing evidence for our hypothesis.

280

### 281 **Metabolic and genomic signature of antagonistic interaction**

282 To understand the mechanisms of antagonistic interaction between figs of *F.*  
283 *pumila* var. *pumila* and larvae of *W. pumilae*, we analyzed chemical profiles of  
284 different tissue types of female and functional male figs at the receptive and the post-  
285 receptive stage using metabolomic data (Supplementary Table 7; see Methods). We  
286 focused on the secondary metabolites associated with plant chemical defenses  
287 (SMCDs)<sup>22,37-39</sup>, comprising some terpenoids (triterpenes and sesquiterpenes) and  
288 phenylpropanoids (including their precursors and their derivatives) (Supplementary  
289 Fig. 12). Metabolomic analysis revealed 736 SMCDs (108 terpenoids and 628  
290 phenylpropanoids) (Supplementary Table 15). While we found significant differences  
291 in chemical profiles between two types of tissues and between different fig  
292 development stages, there were few differences between female and functional male  
293 figs (Fig. 4a). No secondary metabolites with significant difference in quantity  
294 (SMSDs) were found between feeder and seed florets at the receptive stage, and there  
295 were only three SMSDs between galled ovules and seeds at the post-receptive stage

296 (Fig. 4b). Remarkably, we found similar changes of SMSDs in both the feeder floret-  
297 galled ovule and the seed floret-seed transitions (Fig. 4c and Supplementary Fig. 13a).  
298 Besides SMCDs, galled ovules and seeds shared similar overall chemical profiles  
299 (Supplementary Fig. 14). These results showed similar chemical changes and profiles  
300 in the development of female florets no matter they were parasitized by pollinator  
301 larvae (becoming galled ovules) or not (developing into seeds).

302 As might be expected from organisms that spend most their lives in a specific  
303 environment, contraction of three gene families crucial to the detoxification of plant  
304 defensive chemicals<sup>40</sup> (CYP450s, glutathione s-transferases (GSTs) and  
305 carboxylesterases (CCEs) gene families) was found in the genomes of *W. pumilae*, *E.*  
306 *verticillata* and *C. solmsi* (Fig. 4d and Supplementary Fig. 15). Such contraction was  
307 mainly caused by gene loss and infrequent tandem duplication (Supplementary Fig.  
308 7b-d), and most of the detoxification-related genes in the three pollinating wasp  
309 species were in the same monophyletic groups (Supplementary Fig. 16). Ten out of  
310 the 56 detoxification-related genes in *W. pumilae* was at a high level (read counts >  
311 200) and was significantly upregulated at the larval stage compared to the adult stage  
312 (Supplementary Fig. 17 and Supplementary Table 16). These metabolic and genomic  
313 signatures provide a molecular basis for further exploring the mechanisms of fig-  
314 pollinator coadaptation during their antagonistic interaction.

## 315 **Discussion**

316 Reciprocal selection on signaling and defense traits has shaped the molecular  
317 constraints governing how antagonistic larvae develop into mutualistic adult

318 pollinators<sup>8,41</sup>. In this study, our novel combination of classic electrophysiological  
319 experiments and multi-omics approaches has illuminated some key mechanisms  
320 forming the coadaptation in a pair of fig-pollinator mutualists. We identified the  
321 attractive VOC, detected that host identification by the specific pollinators may be  
322 linked to their reduced number of OBP genes, and validated an OPB mainly binding  
323 the attractant. We identified the key genes involved in the regulation of both attractant  
324 and repellent biosynthesis in the plant: from facilitating the synthesis of the repellent  
325 to favoring the production of the attractant. Surprisingly, matched changes in SMCDs  
326 occurred across the transitions from i) floret to galled ovule and ii) floret to seed, and  
327 almost identical profiles of SMCDs were found in galled ovules and seeds. As for the  
328 pollinator, we detected a contraction of detoxification-related gene families.

329       Previous studies have mainly focused on the dominant components or the  
330 bouquet of components in the VOCs emitted by figs<sup>14,17</sup>. In contrast our results  
331 showed that only one VOC of relative low concentration attracts the focal pollinating  
332 wasp species, addressing the importance of detailing the complete spectrum of VOCs.  
333 Moreover, the attractive VOC (an aldehyde) in our focal species is distinct from the  
334 attractants found in other *Ficus* species (usually terpenes)<sup>11,13,14,17,18</sup>. Such a dramatic  
335 difference indicates deep divergence among congeners in the recognition of VOC  
336 attractants<sup>42,43</sup>, providing the basis for adaptive radiations in both *Ficus* and their  
337 pollinating wasps<sup>44</sup>. In addition, similar concentration of the attractant emitted by  
338 different sexes of figs supports the intersexual mimicry hypothesis in *Ficus* species<sup>21</sup>,  
339 which argues that any changes in biosynthesis of attractant VOCs in female figs may

340 cause loss of sexual reproduction<sup>21</sup>.

341       Similar chemical changes in the development of galled ovules and seeds and  
342 almost identical SMCD profiles in these tissues showed that the occupancy of  
343 pollinator larvae activates the reproductive program of galled ovules. This suggests  
344 that galling strategy may help pollinator larvae avoid the potential chemical sanctions  
345 when they exploit nutrients of host plants. This is likely to result from either pollinator  
346 larvae manipulating plant physiology or changes triggered by host figs once the feeder  
347 florets are galled. Chemical mimicry of fruits and seeds has been reported in other  
348 galling insects<sup>24,25</sup>, while many studies also suggest that figs have evolved to  
349 accommodate pollinator larvae<sup>10,15</sup>. Other possibilities, such as pollination before  
350 oviposition combined with minimal initial interference of pollinator larvae can be  
351 largely excluded, because most galled ovules were not pollinated (Wang R., personal  
352 observations). Furthermore, we collected figs at the middle (four weeks after the  
353 entrance of pollinator foundresses) of the post-receptive stage (generally lasting 8-10  
354 weeks). Future research should perform bioassays to determine the chemicals  
355 inducing the development of galled ovules and the specific secondary metabolites  
356 defending against pollinator larvae. This will reveal how pollinator larvae activate the  
357 reproductive programs of host plants and why they can only utilize feeder florets.

358       The pollinating wasp species have evolved specializations in OBP and  
359 detoxification-related genes, probably because they are host specific and spend most  
360 of their lives inside galled ovules (though some detoxification-related genes are not  
361 only involved in detoxification but also important for the general life cycle of insects).

362 Such specializations facilitate the maintenance of host-specificity, but conservation of  
363 some OBP genes among pollinating wasps (Supplementary Figs. 6, 7) may also offer  
364 opportunities for host shift<sup>19,45,46</sup>. Moreover, selection to maximize pollinator fitness  
365 may drive rapid adaptive changes in fig traits like floral scents, and such reciprocal  
366 selection has occurred in some generalized plant-pollinator systems<sup>47</sup>.

367 Ongoing global changes are causing rapid evolution and phenotypic changes in  
368 many plants, leading to mismatches between key traits bridging plants and their  
369 pollinators<sup>4,48</sup>. Erosion of these links can result in the collapse of long-evolved  
370 mutualisms and a loss of biodiversity, but may also lead to the rewiring of host  
371 association networks<sup>4,49,50</sup>. Limitations to our knowledge of molecular determination  
372 in plant-pollinator interactions have made predictions about future changes in  
373 biodiversity and ecosystem functioning largely speculative. Our findings offer an  
374 example of gene for gene coadaptation that extends beyond the existing phenotype-  
375 based models of mutualism persistence<sup>51</sup> and place trait-based multi-omics at the  
376 center of the ecological and evolutionary research concerning interacting species in  
377 more diffuse systems.

378

## 379 **ACKNOWLEDGMENTS**

380 We thank Yong-Jin Wang, Qi-Chong Zhu, Qiong Sun, Qian-Ya Li, Jing-Wen Wang,  
381 Tong-Lei Xu, Yue Chen, Fang-Lu Wei, Guo-Chun Shen, Xiu-Lian Wen and Li-Sha Li  
382 for their kind helps in field experiments, Xiu-Lian Wen, Li-Sha Li and the Public  
383 Technology Service Center of XTBG (CAS) for assisting active VOCs analysis, and

384 Xiu-Guang Mao, Pan-Yu Hua and Da-Yong Zhang for constructive suggestions in  
385 data analysis. This work is supported by NSFC grants 31630008 and 31870356 (X.-  
386 Y.C.), and 31870359 (G.W.); and a Talents 1000 Fellowship of Shaanxi Province  
387 (D.D.). S.S. acknowledges departmental support from Harper Adams University.

388

### 389 **Author contributions**

390 X.-Y.C. and R.W. conceived and designed the study. R.W., Y.Yang., S.G.C., S.S., H.Y.  
391 and Z.Y conducted the experiments and analyzed data. Y.J., Q.F.L., H.Y., Y.Z., G.W.,  
392 J.C., R.M., S.C., Y.C., D.D., H.Q.L., M.L., Y.-Y.D., Y.-Y.L, X.T., P.W., J.J.Y., X.-T.Z.,  
393 Q.G., J.-Y.Y., Y.Yin, K.J., and H.M.Y. contributed to data acquisition and data  
394 analyses. R.W., S.S., S.G.C., J.Q.L., J.-Y.R., F.K., C.A.M, A.C., P.M.G, Y.-Y.Z. and  
395 X.-Y.C. edited the manuscript. All authors contributed to writing the manuscript.

396

### 397 **Competing interests**

398 The authors declare no competing interests.

399

### 400 **Data availability**

401 The data that support the findings of this study have been deposited in the CNSA  
402 (<https://db.cngb.org/cnsa/>) of CNGBdb with accession code CNP0000674.

403

### 404 **Methods**

405 **Genome assembly and annotation.** Genomic DNA was extracted from leaves of a  
406 female *F. pumila* var. *pumila* individual nearby Zhejiang Tiantong Forest Ecosystem

407 National Observation and Research Station (TINAS) (E 121°47', N 29°48'), Ningbo,  
408 China, and from c. 500 adult female pollinators of *W. pumilae* emerged from five figs  
409 on a functional male tree in South China Botanic Garden (SCBG) (E 113°11', N  
410 23°11'), Guangzhou, China. Six pair-end and mate-pair libraries were prepared with  
411 varying insert sizes (Supplementary Table 1) for sequencing on an Illumina Hiseq  
412 4000 platform. We also carried out PacBio single-molecule real-time sequencing of  
413 20kb SMRTbell libraries using a PacBio Sequel platform. Based on the Illumina pair-  
414 end sequencing data, the genome sizes of both species were estimated by counting k-  
415 mer frequency using Jellyfish version 2.1.3<sup>52</sup>.

416 *De novo* genome assembly was conducted using MECAT version 1.2<sup>53</sup>. The  
417 initial contig was polished twice based on raw PacBio data and then corrected twice  
418 using Illumina paired-end reads with pilon version 1.22<sup>54</sup>. Redundans version 0.13c<sup>55</sup>  
419 was used to exclude redundant contigs, and we removed contaminative sequences by  
420 searching against the NCBI nucleotide sequences database  
421 (<ftp://ftp.ncbi.nlm.nih.gov/blast/db/FASTA/>) using megablast<sup>56</sup> with e-value  $\leq 1e^{-5}$ .  
422 Gap filling was implemented with PBJelly<sup>57</sup> after scaffolding based on Illumina mate-  
423 pair reads using BESST version 2.2.7<sup>58</sup>.

424 To further improve the quality of genome assembly of both species, we used  
425 high-throughput chromatin conformation capture (Hi-C) technique to scaffold contigs  
426 into pseudo-chromosomes. We constructed Hi-C libraries using the protocol described  
427 by Belton et al.<sup>59</sup>. Fresh leaves sampled from the same *F. pumila* var. *pumila*  
428 individual used in above sequencing and adult female pollinators from SCBG were

429 cross-linked by 4% formaldehyde solution, followed by an overnight digestion with a  
430 4-cutter restriction enzyme MboI (400 units) at 37°C, preparation DNA ends with  
431 biotin-14-dCTP and blunt-end ligation of the cross-linked fragments. Then, the  
432 proximal chromatin DNA was re-ligated by ligation enzyme, and the nuclear  
433 complexes were reverse cross-linked by proteinase K. After that, we extracted and  
434 purified DNA and removed biotin from non-ligated fragment ends using T4 DNA  
435 polymerase. The following steps including end reparation, enrichment of biotin-  
436 labeled Hi-C samples, and ligation by Illumina paired-end (PE) sequencing adapters,  
437 and then the Hi-C library (insert size of 350 bp) was amplified by PCR and sequenced  
438 on an Illumina NovaSeq 6000 platform. High quality data checked by HiC-Pro<sup>60</sup> were  
439 mapped to genome using BWA, with extraction of uniquely mapped reads for pseudo-  
440 chromosome clustering and assembly using Juicer<sup>61</sup> and 3D-DNA<sup>62</sup>.

441       Following genome assembly, we assessed completeness using BUSCO version  
442 3.0.3<sup>63</sup> and Iso-Seq full-length transcripts. The high-quality full-length transcripts  
443 were mapped to genome assemblies using GMAP version 2014-12-21<sup>64</sup>, setting a  
444 cutoff of aligned coverage at 0.85 and aligned identity at 0.9. The quality of genome  
445 assembly was further tested by mapping Illumina paired-end reads to the genome  
446 assemblies using BWA with the depth of coverage calculated using BamDeal version  
447 0.19 (<https://github.com/BGI-shenzhen/BamDeal/>). For each species, Iso-Seq  
448 sequencing was performed using a PacBio Sequel platform, based on two SMRTbell  
449 libraries with insert sizes of 0 - 5kb and 4.5kb - 10kb established by full-length  
450 complementary DNA (cDNA). We used fresh leaves, young stems from fertile and

451 sterile branchlets and figs at different developmental stages for the plant, and adult  
452 males and females for the pollinator.

453 Genome annotation includes repeat identification (including tandem repeats  
454 (TRs) and transposable elements (TEs)), annotation of non-coding RNAs (ncRNA)  
455 and gene prediction and annotation. When annotating repeat sequences, TRs were  
456 identified using Tandem Repeats Finder (TRF) version 4.07<sup>65</sup>, and TEs were searched  
457 against Repbase 21.01<sup>66</sup> and the transposable element protein database using  
458 RepeatMasker version 4.0.6 (<http://www.repeatmasker.org/>) and RepeatProteinMask  
459 in RepeatMasker. LTR\_Finder<sup>67</sup>, PILER<sup>68</sup> and RepeatScout<sup>69</sup> were used to create a *de*  
460 *novo* TE library, and the combined non-redundant library was classified by running  
461 RepeatMasker again.

462 To annotate ncRNAs, tRNAscan-SE version 1.3.1<sup>70</sup> was used to identify tRNA  
463 and their secondary structures. While small nuclear RNA (snRNA) and microRNAs  
464 (miRNAs) were searched for using INFERNAL version 1.1.1<sup>71</sup> in the Rfam database  
465 version 12.0<sup>72</sup>, followed by the detection of rRNAs by aligning with plant or  
466 invertebrate rRNA sequences using BLASTN (E-value  $\leq 1e^{-5}$ ).

467 Gene model prediction was conducted using the MAKER pipeline version  
468 2.31.10<sup>73</sup>. The Iso-Seq full-length transcripts, RNA-seq transcripts (assembled using  
469 Hisat2 version 2.0.1<sup>74</sup> and StringTie version 1.3.3<sup>75</sup>), the protein sequences of related  
470 species and protein sequences from Swiss-Prot database (<https://www.uniprot.org>)  
471 were included in the analysis. Ab-initio gene prediction was performed with the gene  
472 predictors SNAP<sup>76</sup> and AUGUSTUS<sup>77</sup>. The MAKER pipeline was run for two (for the

473 plant) and three (for the pollinator) iterations for training and the final trained hidden  
474 Markov model (HMM) was used for annotation. JBrowse version 1.12.3<sup>78</sup> was used to  
475 examine the gene models following each iteration. The gene models with the presence  
476 of a PFAM domain or with AED  $\leq 0.6$  for *W. pumilae* and AED  $< 1$  for *F. pumila* var.  
477 *pumila* were retained. BUSCO was used to evaluate the completeness of gene  
478 annotation for both genomes.

479 After determining gene models, functions of protein-coding genes were annotated  
480 using DIAMOND version 0.8.23<sup>79</sup> by aligning them to NCBI NR database, Swiss-  
481 Prot<sup>80</sup> and KEGG<sup>81</sup> databases. Motifs and domains in protein sequences were  
482 annotated using InterProScan version 5.16-55.0<sup>82</sup> via searching public databases.  
483 Gene Ontology terms for each gene were assigned using Blast2GO version 3.3<sup>83</sup>.

484 **Comparative genomics.** To analyze the evolutionary characters of our studied  
485 genomes, we first carried out gene family clustering. The genome and annotation data  
486 of 13 other angiosperm species and 11 other arthropod species were downloaded  
487 (Supplementary Table 6). The gene models with open reading frames shorter than  
488 90bp were removed, and only the longest transcript was chosen to represent each  
489 gene. Gene family clustering was performed using OrthoMCL version 10-148<sup>84</sup> for  
490 the plant and TreeFam pipeline version 0.5.1<sup>85</sup> for the pollinator.

491 We then determined the phylogenetic relationships among the plants and among  
492 the insects in the species pools used in gene family clustering. Corresponding coding  
493 sequences (CDSs) were aligned based on the protein sequences of all single-copy  
494 orthologs using MUSCLE version 3.8.31<sup>86</sup>, and codon position 2 of aligned CDSs

495 were concatenated into a super gene using an in-house Perl script with a filtration of  
496 ambiguously aligned positions using trimAI version 1.4.1<sup>87</sup>. After that, phylogenetic  
497 trees were reconstructed using PhyML version 3.0<sup>88</sup> using a GTR substitution model  
498 with a gamma distribution and 100 bootstrap replicates. PAML version 4.9<sup>89</sup> was used  
499 to estimate divergence time, setting 10,000 MCMC generations with a sampling  
500 frequency of 5,000 and a burn-in of 5,000,000 iterations. Overall substitution rate was  
501 assessed using BASEML setting a REV substitution model.

502 Gene family expansion and contraction was analyzed using CAFE version 2.1<sup>90</sup>,  
503 which employed a stochastic birth-and-death process to model the evolution of gene  
504 family sizes over a phylogeny. The birth-and-death parameter ( $\lambda$ ) was estimated using  
505 10,000 Monte Carlo random samples. We then used family-wise method to  
506 statistically test if a gene family experienced significant expansion/contraction, and  
507 gene families with conditional P-values less than 0.05 were considered to have  
508 accelerated rates of gains and losses.

509 We then tested whether the genomes of *F. pumila* var. *pumila* experienced whole  
510 genome duplication (WGD). Syntenic blocks were identified using MCscan version  
511 0.8<sup>91</sup>, and the rate of transversions on fourfold degenerate synonymous sites (4DTV)  
512 was calculated using the HKY substitution model to uncover potential speciation or  
513 WGD events occurring in evolutionary history of the plant. For *W. pumilae*, we tested  
514 for genomic segmental duplications (SDs). The self-alignment was performed using  
515 BLASTZ version 1.02<sup>92</sup>, and a non-redundant set of SDs was obtained using WGAC  
516 version 1.3<sup>93</sup>.

517 **Annotation of specific gene families and analysis of their evolution.** To test  
518 whether the contraction specific gene families in *W. pumilae*, *E. verticillata* and *C.*  
519 *solmsi* contributes to the wasps' host-specificity and detoxification ability, we  
520 conducted a detailed annotation in chemosensory gene families (OBPs, CSPs, ORs  
521 and IRs) and detoxification gene families including CYP450s, GSTs and CCEs. The  
522 homologous genes of *N. vitripennis*, *Apis mellifera* and *Drosophila melanogaster*  
523 were used as queries to search the genome assembly of *W. pumilae* using TBLASTN  
524 at a criterion of E-value  $\leq 1e^{-5}$ , and gene structures of identified genes were predicted  
525 using GeneWise version 2.4.1<sup>94</sup> with pseudogenes masked. We repeated this process  
526 iteratively until no more genes were detected. Additional genes from the MAKER  
527 annotation were also included if they included corresponding InterPro domains. All  
528 gene structures were manually checked and corrected if necessary, on the basis of full-  
529 length transcripts, RNA-seq transcripts and homologous proteins in JBrowse. We used  
530 Binomial Distribution One-tailed test to examine gene family expansion/contraction  
531 among the compared species without considering their evolutionary relationships.

532 To reveal the evolutionary history of OBP, CYP450, CCE and GST gene families,  
533 syntenic blocks were identified across the genomes of the three pollinating wasp  
534 species and *N. vitripennis* using MCscan (<https://github.com/tanghaibao/jcvi/wiki>  
535 /MCscan-(Python-version)). We then constructed neighbor-joining phylogenetic trees  
536 to verify homologous genes among these insect species, using TreeBeST version  
537 1.9.2<sup>95</sup> using a JTT model and 1000 bootstraps.

538 **VOC collection and component analysis.** To reveal the composition of volatile

539 organic compounds (VOCs) emitted by figs of *F. pumila* var. *pumila* at different  
540 developmental stages, we collected VOCs from figs at both pre-receptive and  
541 receptive stages (Fig. 1a) in spring 2018 using dynamic headspace sampling (DHS)  
542 techniques<sup>96</sup>. After a careful search, we chose ten mature *F. pumila* var. *pumila* trees  
543 comprising five females and five functional males (Supplementary Table 8) nearby  
544 TINAS, within the natural range of the plant. Three figs were labeled on each selected  
545 individual. At either fig developmental stage (from early to middle April for pre-  
546 receptive stage and late April for receptive stage), we extracted the VOCs emitted by  
547 each labeled fig into an activated porapak adsorption tube (150 mg) during 8:00-11:00  
548 am, using a protocol identical to Tholl et al. (2006)<sup>96</sup>. Each adsorption tube was then  
549 eluted three times using 300  $\mu$ l n-hexane and stored at -20 °C.

550 VOCs emitted by figs were then separated and identified using a coupled Gas  
551 Chromatography-Mass Spectrometry (GC-MS) system (HP 7890A-5975C, Agilent,  
552 US)<sup>97</sup>. For each sample, 1.8  $\mu$ l of eluate VOC extract, concentrated using nitrogen,  
553 was injected in split mode with a split ratio of 10 : 1 at 250 °C. Helium (1 mL/min)  
554 was used as carrier gas in a HP-5ms (30 m  $\times$  250  $\mu$ m  $\times$  0.25  $\mu$ m, Agilent, US) GC  
555 column. We set the oven ramp at 40°C for 1 min, and then 3 °C/min to 140 °C for 1  
556 min, followed by 5 °C/min to 230 °C for 3 mins. Ionization was conducted by  
557 electron impact (70 eV, source temperature 230 °C). The MS quadrupole was heated  
558 to 150 °C, with the scanned mass range setting as from 40 to 550 m/z. Compound  
559 identification was implemented by matching the mass spectra with NIST 08 MS  
560 libraries. We then calculated the relative proportions of all compounds emitted by figs

561 at each developmental stage.

562 To evaluate the difference in the concentration of decanal between ostiolar tissues  
563 and female florets, we sampled figs at receptive stages from three female and three  
564 functional male individuals and identified the composition of VOCs emitted from  
565 these two types of tissues using the same approach mentioned above. The decanal  
566 concentration in each type of tissues in a plant individual was quantified by  
567 comparing its peak area with the internal standard (decyl acetate).

568 **Electrophysiological responses of pollinating wasps.** To narrow the range of  
569 candidate VOCs attracting *W. pumilae*, we tested the electrophysiological responses of  
570 the pollinators to the collected VOCs, using gas chromatography-electroantennogram  
571 detection (GC–EAD). We used a system coupling a custom-made EAG<sup>98</sup> with a GC  
572 (Trace GC 2000, Thermo Finnigan, US). We injected 1.8 µl of concentrated VOC  
573 extract eluate into the GC to separate different compounds. The GC conditions were  
574 identical to those used for the GC–MS component analysis, except that the oven ramp  
575 was set to 50 °C for 2 mins, and then to 10 °C/min up to 280 °C for 1 min. After GC–  
576 FID (flame ionization detector) quantification, outflow from the GC column was  
577 delivered to the EAG as the stimulus through a custom, 40 cm long heated (at 250 °C)  
578 transfer line with a clean, wet, and static-free airflow. The stimulus was then puffed to  
579 the antenna of an adult female pollinator (collected from figs in TINAS) fixed onto  
580 the EAG with both ends of the antennae connected with prepared glass electrodes  
581 linking the probes of EAG to the potentiometric amplifiers.

582 This experiment was repeated 5 times (i.e. antennae of 5 adult female

583 pollinators), and the EAD signal was recorded using a HP 34465A digital multimeter  
584 (Keysight, US). Both EAD and FID signal data were aligned to verify the tentative  
585 compounds stimulating the adult female pollinator, using the software IO Libraries  
586 Suite 16 (Agilent, US) and BenchVue (Keysight, US). These tentative effective  
587 compounds were identified by matching the chromatographs with the results of  
588 component analysis using GC–MS.

589 We further tested the electrophysiological response of adult female pollinators  
590 (collected from figs in SCBG) to the synthesized standard of each tentative compound  
591 (TIC, JPN; TRC, CAN; Sigma-Aldrich, US), following the same procedures as above.  
592 A compound was determined as truly effective only when it was confirmed by the  
593 experiments using both eluate of VOC extracts and synthesized standard.

594 **Behavioral preference of pollinating wasps.** To test the behavioral preference of *W.*  
595 *pumilae* to different tentative effective VOCs, we used a Y-tube olfactometer (stem 8  
596 cm, arms 9 cm, at an angle of 55°, internal diameter of 1.5 cm) following the methods  
597 described by Wang et al.<sup>19</sup>. We placed the synthesized standard of each tentative  
598 effective VOC in the glass container, connecting one arm of the olfactometer to this  
599 treatment of n-hexane and blends of putative stimuli compounds and the other arm to  
600 the controls (only n-hexane) (Supplementary Table 9). VOCs were passed from both  
601 arms to the stem through equal flow rates of cleaned and humidified airflow created  
602 by an air pump system with an activated charcoal filter and distilled water. To avoid  
603 visual distractions to the pollinators, we placed the olfactometer in the center of a  
604 white table illuminated using three 40-W cool white fluorescent tubes above the arms.

605 Each healthy adult female pollinator (collected from figs in SCBG) was tested  
606 independently with an observation for 5 mins in the olfactometer, and its behavior was  
607 assigned to one of the three choices: (1) towards the treatment (the insect went 1 cm  
608 past the Y junction (decision line) and stayed there more than 1 min); (2) towards the  
609 control; and (3) no choice (the insect did not reach the decision line within 5 mins).  
610 For each treatment-control combination, we repeated this experiment 50 times (i.e. 50  
611 adult female pollinators) and compared the proportions of different choices (towards  
612 the treatment and towards the control) using GLMs assuming binomial distribution of  
613 residuals to examine the preference of *W. pumilae*.

614 **Sample collection for comparative transcriptome, proteome and metabolome.** To  
615 reveal the molecular mechanisms forming the specific pollinator-host identification  
616 based on both transcriptomic and proteomic data, in spring 2017 and 2018, after  
617 collecting several pre-receptive and receptive figs from the ten mature individuals of  
618 the plants used in VOCs collection (Supplementary Table 7), we dissected each  
619 sampled fig to gather ostiolar tissues with bracts and female florets. The total sample  
620 size therefore was 40 for the plant (a type of tissues collected from a single tree at  
621 each fig developmental stage is one sample, with 20 samples for each type of tissues).  
622 In spring 2018, we sampled at least 5 figs at the mature stage from each of the five  
623 functional male mature individuals used for VOC collection (Supplementary Table 7).  
624 Each sampled mature fig was dissected into halves in a Teflon bag, and then each half  
625 was rapidly moved into a Teflon bag containing only clean air filtered by activated  
626 charcoal (as a control) or clean air and a receptive fig (as a treatment), to test whether

627 differential expression occurred in some chemosensory genes when adult females  
628 were exposed to attractive VOCs. We then collected all adult females of *W. pumilae*  
629 emerging from the sampled figs according to the identity of functional male trees (a  
630 total of 10 samples with at least 100 adult female wasps in each sample). All sampled  
631 fig tissues and adult female pollinators were first stored in liquid nitrogen for 72 hours  
632 and then moved into a refrigerator at -80 °C.

633 To unravel how pollinator larvae adapt to the environments inside galled ovules  
634 using metabolomes, we sampled several receptive and post-receptive figs from the ten  
635 plant individuals (Supplementary Table 7) and collected ostiolar tissues (20 samples),  
636 female florets (10 samples), galled ovules (5 samples) and seeds (5 samples) in spring  
637 2020. For clearly distinguishing galled ovules and seeds from the female florets that  
638 were neither pollinated nor utilized by pollinators, the post-receptive figs were  
639 sampled four weeks after the entrance of adult female pollinators.

640 **RNA-seq for *F. pumila* var. *pumila* and *W. pumilae*.** After generating PCR-based  
641 libraries and sequencing on a BGISEQ500 platform (BGI, CHN), low quality reads  
642 were filtered using SOAPnuke version 1.5.6<sup>99</sup>. The acquired clean reads were then  
643 mapped to the genome assemblies of our studied species using Bowtie version 2.2.5<sup>100</sup>  
644 and gene expression were quantified by RSEM version 1.2.12<sup>101</sup>.

645 **Quantitative proteomes for *F. pumila* var. *pumila* and *W. pumilae*.** We identified  
646 and quantified proteins for ostiolar tissues (sampled in 2017) using iTRAQ (isobaric  
647 tags for relative and absolute quantitation)-based method. The strategy of quantifying

648 proteomes was conducted according to the methods described by Tian et al. (2013)<sup>102</sup>.  
649 After total protein extraction, peptide labeling was performed using an iTRAQ  
650 Reagent 8-plex Kit according to the manufacturer's protocol. Extraction was followed  
651 by peptide fractionation, and the peptides separated from LC-20AD nano-HPLC  
652 (Shimadzu, JPN) were transferred into the tandem mass spectrometry Q EXACTIVE  
653 (MS/MS) (Thermo Fisher Scientific, US) for data-dependent acquisition (DDA)  
654 detection. After converting the raw MS/MS data into MGF format using Proteome  
655 Discoverer version 1.2 (Thermo Fisher Scientific, US), the exported data in MGF  
656 format were searched using Mascot version 2.3 (Matrix Science, US) against the  
657 protein-coding sequences from our gene prediction. Quantification of proteins was  
658 achieved using IQuant<sup>103</sup>, which uses the Mascot Percolator algorithm<sup>104</sup> to improve  
659 the results of peptide identification and the principle of parsimony to assemble  
660 proteomes. All the proteins with a false discovery rate (FDR)<sup>105</sup> of less than 1% were  
661 retained for further analyses.

662 We used a DIA (data independent acquisition) approach to identify and quantify  
663 proteins in female florets and adult female pollinators (collected in 2018). Procedures  
664 identical to iTRAQ were first performed on the total protein extraction, peptide  
665 fractionation and peptides separation. Then, to create reference spectra for DIA, we  
666 first conducted DDA on a Q-EXACTIVE HF mass spectrometer (Thermo Fisher  
667 Scientific, US) coupled with an Ultimate 3000 RSLCnano system (Thermo Fisher  
668 Scientific, US) after a further peptide separation on an in-house packed nano-LC  
669 column (150  $\mu\text{m}$   $\times$  30 cm, 1.8  $\mu\text{m}$ , 100  $\text{\AA}$ ). Then, using the same instruments, DIA

670 was performed following a brief procedure that consisted of a survey scan at 120,000  
671 resolution from 400 to 1,250 m/z (MIT 50 ms), followed by scanning in DIA isolation  
672 windows setting 17 m/z with loop count 50 at 30,000 resolution (automatic gain  
673 control target  $3 \times 10^6$  and auto MIT). The DDA spectra were identified by searching  
674 against the database of protein-coding sequences using the MaxQuant version 1.5.3.30  
675 <sup>106</sup>(Cox and Mann, 2008) at the FDR level of 1% with the minimum peptide length of  
676 7. Based on the spectrogram database of DDA spectra, peptides and proteins in DIA  
677 data were identified and quantified using Spectronaut<sup>107</sup>, employing the mProphet  
678 approach and setting iRT for retention time prediction. A target-decoy model was used  
679 to verify the quantification results at an FDR level of 1%.

680 **Measurement of metabolomes of different types of tissues.** Chromatographic  
681 separation of metabolites was performed using an Ultra-Performance Liquid  
682 Chromatography (UPLC) System (Waters, UK), with an ACQUITY UPLC HSS T3  
683 column (100mm\*2.1mm, 1.8 $\mu$ m) (Waters, UK) being used for the reversed phase  
684 separation and setting oven temperature at 50° C and flow rate of 0.4 ml/min. After  
685 separation, gradient elution was conducted as following procedure: 0~2 min, 100%  
686 mobile phase A (water + 0.1% formic acid); 2~11 min, 0% to 100% mobile phase B  
687 (acetonitrile + 0.1% formic acid); 11~13 min, 100% B; 13~15 min, 0% to 100% A.  
688 The injection volume for each sample was 10  $\mu$ l. Then, the eluted metabolites were  
689 identified in both positive and negative ion modes using a high-resolution tandem  
690 mass spectrometer Xevo G2 XS QTOF (Waters, UK). The capillary and sampling  
691 cone voltages were set at 3.0 kV and 40.0 V for positive ion mode and at 2.0 kV and

692 40.0 V for negative ion mode. Mass spectrometry data were acquired in Centroid  
693 MSE mode, setting the TOF mass range from 50 to 1200 Da and the scan time of 0.2  
694 s. For MS/MS detection, all precursors were fragmented at 20-40 eV with the scan  
695 time of 0.2 s. A quality control (QC) sample (pooling all samples together) was used  
696 after every 10 samples. Peak alignment, peak picking and quantitation of each  
697 metabolite were performed using Progenesis QI version 2.2, and the quality control  
698 based on LOESS signal correction<sup>108</sup> was conducted using QC samples.

699 **Comparative transcriptome, proteome and metabolome analysis.** We carried out  
700 differential expression/concentration analysis for transcriptomes, proteomes and  
701 metabolomes. This allowed us to anchor the key genes contributing to the attractant-  
702 induced host specificity and adaptation of pollinator larvae to plant chemical defenses.

703 For transcriptomes, differential expression were tested between ostiolar tissues  
704 and female florets (feeder and seed florets)/galled ovules/seeds at each of the three fig  
705 developmental stages (pre-receptive, receptive and post-receptive stages), and in  
706 either type of fig tissues between any two of these three stages and between sexes at  
707 each stage. For the pollinator, differential expression was conducted between  
708 contacting attractive VOC(s) vs. not contacting and between adults and larvae. We  
709 performed comparisons using DEseq2 version 1.4.5<sup>109</sup> based on negative binomial  
710 distributions. *P*-values were corrected using a Benjamini-Hochberg (BH) method for  
711 multiple tests. The differentially expressed genes (DEGs) with a fold change  $\geq 2$  and  
712 an adjusted *p*-value  $\leq 0.05$  were considered as statistically significant.

713 For proteomes, in ostiolar tissues, we tested the proteins with significant

714 difference in quantity (PSDs) between the pre-receptive and the receptive stages and  
715 between sexes at each stage using IQuant, and PSDs were defined as fold changes in  
716 protein abundance  $\geq 1.2$  and Q-value  $\leq 0.05$ . In female florets and adult female  
717 pollinators, PSDs were analyzed using MSstats<sup>110</sup> at criterions of fold changes  $\geq 2$  and  
718 Q-value  $\leq 0.05$ .

719 For metabolomes, to examine whether there were significant differences in  
720 profile of secondary metabolites associated with chemical defenses (SMCDs) between  
721 different types of tissues and between the receptive and the post-receptive stages, we  
722 first carried out enrichment analysis to enrich all relevant secondary metabolites into  
723 the pathways associated with plant chemical defenses and then clustered all samples  
724 into different categories using PLS-DA model in metaX<sup>111</sup>. Data were log<sub>2</sub>-  
725 transformed and scaled by Pareto scaling. Secondary metabolites with significant  
726 difference in quantity (SMSDs) were defined as VIP (variable importance for the  
727 projection calculated based on the first two axes from PLS-DA model)  $\geq 1$ , fold  
728 change  $\geq 1.2$  or  $\leq 0.83$  and Q-value  $\leq 0.05$ . In addition, we performed PLS-DA model  
729 to test the difference in the entire profile of secondary metabolites between different  
730 types of tissues and between different fig developmental stages.

731 **Motif analysis.** We conducted motif analysis to check whether the OBPs in the same  
732 syntenic blocks among the three pollinating wasp species have similar motif structure  
733 using MEME Suite 5.0.4<sup>112</sup>. Motifs with E-value  $\leq 0.05$  were used for inter-specific  
734 comparisons. To predict the most likely OBPs related to the identification of specific  
735 attractant and repellent, we created a dataset consisting of all OBPs in *W. pumilae* and

736 the specific OBPs that had been verified to bind to decanal and nonanal in  
737 *Adelphocoris lineolatus*<sup>33</sup> and *Culex quinquefasciatus*<sup>34</sup> as references, and performed  
738 motif analysis.

739 ***In vitro* functional characterization of key genes.** The full-length of open reading  
740 frame (ORF) of the four key genes (for the plant) and of the two OBPs (for the  
741 pollinator) (Supplementary Table 17) was confirmed by RT-PCR and was then cloned  
742 into pET-28a (MilliporeSigma, US). After checking sequences by Sanger sequencing,  
743 these genes were expressed in *E. coli* strains BL21 (DE3) and Rosetta (DE3). The  
744 recombinant proteins produced were purified (purity > 90%) using modified nickel-  
745 nitrilotriacetic acid agarose (Thermo Fisher Scientific, US).

746 We measured the affinities of the two OBPs to different substrates using surface  
747 plasmon resonance (SPR) on a Biacore T200 system (GE Healthcare). OBPs were  
748 reconstituted in sterile PBS and were diluted in 10mM sodium acetate trihydrate (pH  
749 = 4.5) to the concentration of 20ug/ml. Then, each OBP was immobilized by the  
750 amine coupling method on a CM5 sensor chip according to the manufacturer's  
751 protocol (GE Healthcare). Analytes (decanal and nonanal) were diluted in running  
752 buffer (5% DMSO-PBS-P) to the concentration ranging from 0 to 1000  $\mu$ M and were  
753 injected through channels at a flow rate of 20  $\mu$ l/min. Using BIAevaluation (GE  
754 Healthcare), both steady state affinity model and 1:1 binding model were performed  
755 to quantify the binding affinity ( $K_D$ ).

756 For enzyme activity assays of the four key genes of the plant, we used the  
757 reaction system (500  $\mu$ l) mainly composed of 50 mM Tris-HCl (pH 7.4), 0.4~1.0 mM

758 substrate(s) (Supplementary Table 17), 2M dimethyl sulfoxide (for the ADH and the  
759 ALDH)/10% triton X-100 (for the two ASCLs), and 10 µl of purified protein (0.2  
760 mg/ml). After 60 min of incubation at room temperature, we collected the reaction  
761 products by headspace solid-phase microextraction for the ALDH and the ADH  
762 (which were analyzed by GC–MS) and by extraction using diethyl ether for the two  
763 ACSLs (which were analyzed by LC–MS). These experiments were repeated for three  
764 time. In addition, three replications of negative controls (only adding the substrates and  
765 bovine serum albumin) were conducted, and no reaction products were detected.

766 **Cis-element detection and co-expression network analysis.** To test the regulatory  
767 mechanisms in the biosynthesis of attractant and repellent emitted by figs of *F. pumila*  
768 var. *pumila*, we first scanned the binding motifs present in the 2-kb promoter  
769 sequences upstream of key plant genes using PlantCARE<sup>116</sup>. Then, weighted  
770 undirected co-expression networks were conducted using the R package WGCNA<sup>113</sup>  
771 with a soft thresholding power of 8. Modules containing genes with correlated  
772 expression patterns were identified by gene clustering based on the topological  
773 overlap matrix<sup>114</sup> and by cutting the resulting dendrogram using the cutreeDynamic  
774 approach in the R package The Dynamic Tree Cut<sup>115</sup>. Genes with kME values larger  
775 than 0.95 were selected as hub genes. We checked whether some modules containing  
776 both some key plant genes and the transcription factors predicted to bind to them. This  
777 allowed us to uncover the likely regulatory mechanisms.

778 **ChIP-qPCR.** The open reading frame of each of the four transcription factors

779 (*FpumHD-ZIP1*, *FpumHD-ZIP2*, *FpumbZIP1* and *FpumbHLH1* (Supplementary  
780 Table 13)) was cloned into the pET-28a to generate the fusion plasmid encoding the 6  
781 His-tagged fusion protein. This plasmid was transformed into *E. coli* strain Rosetta  
782 (DE3), which were cultured and induced by 0.8 mM isopropyl- $\beta$ -D-thiogalactoside  
783 (IPTG) at 37 °C. The induced cells were then sonicated for supernatant collection, and  
784 the purified recombinant proteins were obtained using a His-tag Protein Purification  
785 Kit (Beyotime Biotechnology, CHN). The purified proteins were used to immunize  
786 rabbits for 52 days to acquire polyclonal antibody (ABclonal Biotechnology, CHN).  
787 We successfully obtained the qualified antibodies for all the four transcription factors  
788 for ChIP-qPCR experiments.

789 ChIP-qPCRs were then conducted for the two transcription factors with qualified  
790 antibodies to examine if it can bind the putative target genes by model prediction. The  
791 ChIP assay was performed based on the protocols described in Gendrel et al.,  
792 (2005)<sup>117</sup>. Approximately 3.0 g ostiolar tissues from figs at receptive stages were  
793 treated using 1% formaldehyde to crosslink and fix the DNA-protein complexes. The  
794 cells of sampled tissues were lysed, and each antibody was used to immunoprecipitate  
795 the antigen transcription factor with its binding DNA fragments. The DNA in the ChIP  
796 products was applied in qPCR with primer pairs designed for the promoters of  
797 putative target genes in a QuantStudio™ 5 real-time PCR detection system (Thermo  
798 Fisher Scientific, US). Each qPCR reaction was performed in triplicates, and the cycle  
799 thresholds (Cts values) of ChIP products were compared with those of input samples  
800 and negative controls (only using IgG) for calculating % input and fold enrichment (%).

801 input (ChIP)/ % input (negative control)). We failed to obtain the Ct values for  
802 negative controls by the end of 35 qPCR cycles, and we therefore used the Ct value of  
803 35 for each negative control when calculating % input and fold enrichment.

804

#### 805 **Additional information**

806 All supplemental figures and tables are included in supplementary information.

807

#### 808 **References**

- 809 1. Lamichhaney, S. et al. Evolution of Darwin's finches and their beaks revealed by  
810 genome sequencing. *Nature* **518**, 371–375 (2015).
- 811 2. Simões, M. et al. The evolving theory of evolutionary radiations. *Trends Ecol.*  
812 *Evol.* **31**, 27–34 (2016).
- 813 3. Arnegard, M. E. et al. Genetics of ecological divergence during speciation.  
814 *Nature* **511**, 307–311 (2014).
- 815 4. Hoffmann, A. A. & Sgrò, C. M. Climate change and evolutionary adaptation.  
816 *Nature* **470**, 479–485 (2011).
- 817 5. Olsen, J. L. et al. The genome of the seagrass *Zostera marina* reveals angiosperm  
818 adaptation to the sea. *Nature* **530**, 331–335 (2016).
- 819 6. Bécerra, J. X., Nogueb, K. & Venable, D. L. Macroevolutionary chemical  
820 escalation in an ancient plant–herbivore arms race. *Proc. Natl. Acad. Sci. USA*  
821 **106**, 18062–18066 (2009).
- 822 7. Edger, P. P. et al. The butterfly plant arms-race escalated by gene and genome

- 823 duplications. *Proc. Natl. Acad. Sci. USA* **112**, 8362–8366 (2015).
- 824 8. Adler, L. S. & Bronstein, J. L. Attracting antagonists: does floral nectar increase  
825 leaf herbivory? *Ecology* **85**, 1519–1526 (2004).
- 826 9. McCall, A. C. & Irwin, R. E. Florivory: the intersection of pollination and  
827 herbivory. *Ecol. Lett.* **9**, 1351–1365 (2006).
- 828 10. Cook, J. M. & Rasplus, J.-Y. Mutualists with attitude: coevolving fig wasps and  
829 figs. *Trends Ecol. Evol.* **18**, 241–248 (2003).
- 830 11. Zhang, X. et al. Genomes of the banyan tree and pollinator wasp provide insights  
831 into fig-wasp coevolution. *Cell* **183**, 1–15 (2020).
- 832 12. Herre, E. A., Jandér, K. C. & Machado, C. A. Evolutionary ecology of figs and  
833 their associates: recent progress and outstanding puzzles. *Annu. Rev. Ecol. Evol.*  
834 *Syst.* **39**, 439–458 (2008).
- 835 13. Souza, C. D. et al. Diversity of fig glands is associated with nursery mutualism in  
836 fig trees. *Am. J. Bot.* **102**, 1564–1577 (2015).
- 837 14. Souto-Vilarós, D. et al. Pollination along an elevational gradient mediated both by  
838 floral scent and pollinator compatibility in the fig and fig-wasp mutualism. *J.*  
839 *Ecol. Evol.* **106**, 2256–2273 (2018).
- 840 15. Wang, R. et al. Loss of top-down biotic interactions changes the relative benefits  
841 for obligate mutualists. *Proc. R. Soc. B.* **286**, 20182501 (2019).
- 842 16. Mori K. et al. Identification of RAN1 orthologue associated with sex  
843 determination through whole genome sequencing analysis in fig (*Ficus carica* L.).  
844 *Sci. Rep.* **7**, 41124 (2017).

- 845 17. Proffit M. et al. Chemical signal is in the blend: bases of plant-pollinator  
846 encounter in a highly specialized interaction. *Sci. Rep.* **10**, 10071 (2020).
- 847 18. Chen, C. et al. Private channel: a single unusual compound assures specific  
848 pollinator attraction in *Ficus semicordata*. *Funct. Ecol.* **23**, 941–950 (2009).
- 849 19. Wang, G., Cannon, C. H. & Chen, J. Pollinator sharing and gene flow among  
850 closely related sympatric dioecious fig taxa. *Proc. R. Soc. B.* **283**, 20152963  
851 (2016).
- 852 20. Yu, H. et al. De novo transcriptome sequencing in *Ficus hirta* Vahl. (Moraceae) to  
853 investigate gene regulation involved in the biosynthesis of pollinator attracting  
854 volatiles. *Tree Genet. Genomes* **11**, 91 (2015).
- 855 21. Soler, C. C. L., Proffit, M., Bessière, J.-M., Hossaert -McKey, M. & Schatz, B.  
856 Evidence for intersexual chemical mimicry in a dioicous plant. *Ecol. Lett.* **15**,  
857 978–985 (2012).
- 858 22. Volf, M. et al. Community structure of insect herbivores is driven by  
859 conservatism, escalation and divergence of defensive traits in *Ficus*. *Ecol. Lett.*  
860 **21**, 83–92 (2018).
- 861 23. Martinson, E.O., Hackett, J.D., Machado, C.A. & Arnold A.E. Metatranscriptome  
862 analysis of fig flowers provides insights into potential mechanisms for mutualism  
863 stability and gall induction. *PLoS ONE* **10**, e0130745 (2015).
- 864 24. Zhang, H. et al. Leaf-mining by *Phyllonorycter blancardella* reprograms the host-  
865 leaf transcriptome to modulate phytohormones associated with nutrient  
866 mobilization and plant defense. *J. Insect Physiol.* **84**, 114–127 (2016).

- 867 25. Schultz, J.C., Edger, P.P., Body, M. & Appel, H.M. A galling insect activates plant  
868 reproductive programs during gall development. *Sci. Rep.* **9**, 1833 (2019).
- 869 26. The *Nasonia* Genome Working Group. Functional and evolutionary insights from  
870 the genomes of three parasitoid *Nasonia* species. *Science* **327**, 343–348 (2010).
- 871 27. Xiao, J.-H. et al. Obligate mutualism within a host drives the extreme  
872 specialization of a fig wasp genome. *Genome Biol.* **14**, R141 (2013).
- 873 28. Ohri, D. & Khoshoo, T. N. Nuclear DNA contents in the genus *Ficus* (Moraceae).  
874 *Plant Syst. Evol.* **156**, 1–4 (1987).
- 875 29. Chen, Y., Compton, S. G., Liu, M. & Chen, X.-Y. Fig trees at the northern limit of  
876 their range: the distributions of cryptic pollinators indicate multiple glacial  
877 refugia. *Mol. Ecol.* **21**, 1687–1701 (2012).
- 878 30. Chen, L.-G. et al. Binding affinity characterization of an antennae-enriched  
879 chemosensory protein from the white-backed planthopper, *Sogatella furcifera*  
880 (Horváth), with host plant volatiles. *Pestic. Biochem. Phys.* **152**, 1–7 (2018).
- 881 31. Gu, S.-H. et al. Functional characterization and immunolocalization of odorant  
882 binding protein 1 in the lucerne plant bug, *Adelphocoris lineolatus* (GOEZE).  
883 *Arch. Insect Biochem.* **77**, 81–98 (2011).
- 884 32. Leal, W. S. et al. Reverse and conventional chemical ecology approaches for the  
885 development of oviposition attractants for *Culex* mosquitoes. *PLoS ONE* **3**, e3045  
886 (2008).
- 887 33. Rizzo, W. B. et al. Fatty aldehyde and fatty alcohol metabolism: review and  
888 importance for epidermal structure and function. *BBA-Mol. Cell Biol. L.* **1841**,

- 889 377–389 (2014).
- 890 34. Schwab, W., Davidovich-Rikanati, R. & Lewinsohn, E. Biosynthesis of plant-  
891 derived flavor compounds. *Plant J.* **54**, 712–732 (2008).
- 892 35. Capella, M., Ribone, P. A., Arce, A. L. & Chan, R. L. *Arabidopsis thaliana*  
893 HomeoBox 1 (AtHB1), a Homeodomain-Leucine Zipper I (HD-Zip I) transcription  
894 factor, is regulated by PHYTOCHROME-INTERACTING FACTOR 1 to  
895 promote hypocotyl elongation. *New Phytol.* **207**, 669–682 (2015).
- 896 36. Jiang, W. et al. Two transcription factors TaPpm1 and TaPpb1 co-regulate  
897 anthocyanin biosynthesis in purple pericarps of wheat. *J. Exp. Bot.* **69**, 2555–  
898 2567 (2018).
- 899 37. Guan, R. et al. Draft genome of the living fossil *Ginkgo biloba*. *GigaScience* **5**,  
900 49 (2016).
- 901 38. Mithöfer, A., & Boland, W. Plant defense against herbivores: chemical aspects.  
902 *Annu. Rev. Plant Biol.* **63**, 431–450 (2012).
- 903 39. Salazar, D. et al. Origin and maintenance of chemical diversity in a species-rich  
904 tropical tree lineage. *Nat. Ecol. Evol.* **2**, 983–990 (2018).
- 905 40. Després, L., David, J. P. & Gallet, C. The evolutionary ecology of insect  
906 resistance to plant chemicals. *Trends Ecol. Evol.* **22**, 298–307 (2007).
- 907 41. Segar, S. T., Volf, M., Sisol, M., Pardikes, N. & Souto-Vilarós, A. D. Chemical  
908 cues and genetic divergence in insects on plants: conceptual cross pollination  
909 between mutualistic and antagonistic systems. *Curr. Opin. Insect Sci.* **32**, 83–90  
910 (2019).

- 911 42. Cook, J. M. & Segar, S. T. Speciation in fig wasps. *Ecol. Entomol.* **35**, 54–66  
912 (2010).
- 913 43. Cruaud, A. et al. An extreme case of plant-insect codiversification: figs and fig-  
914 pollinating wasps. *Syst. Biol.* **61**, 1029–1047 (2012).
- 915 44. Yu, H. et al. Multiple parapatric pollinators have radiated across a continental fig  
916 tree displaying clinal genetic variation. *Mol. Ecol.* **28**, 2391–2405 (2019).
- 917 45. Satler, J. D. et al. Inferring processes of coevolutionary diversification in a  
918 community of Panamanian strangler figs and associated pollinating wasps.  
919 *Evolution* **73**, 2295–2311 (2019).
- 920 46. Wang, G. et al. Genomic evidence of prevalent hybridization throughout the  
921 evolutionary history of the fig-wasp pollination mutualism. *Nat. Commun.* **12**,  
922 718 (2021).
- 923 47. Hoballah, M. E. et al. Single gene-mediated shift in pollinator attraction in  
924 *Petunia*. *Plant Cell* **19**, 779–790 (2007).
- 925 48. Potts, S. G. et al. Global pollinator declines: trends, impacts and drivers. *Trends*  
926 *Ecol. Evol.* **25**, 345–353 (2010).
- 927 49. Kiers, E. T., Palmer, T. M., Ives, A. R., Bruno, J. F. & Bronstein, J. L. Mutualisms  
928 in a changing world: an evolutionary perspective. *Ecol. Lett.* **13**, 1459–1474  
929 (2010).
- 930 50. Segar, S. T., Fayle, T. M., Srivastava, D. S., Lewinsohn, T. M., Lewis, O. T.,  
931 Novotny, V., Kitching, R. L. & Maunsell, S. C. The role of evolution in shaping  
932 ecological networks. *Trends Ecol. Evol.* **35**, 454–466 (2020).

- 933 51. Stoy, K. S., Gibson, A. K., Gerardo, N. M. & Morran, L. T. A need to consider the  
934 evolutionary genetics of host-symbiont mutualisms. *J Evol. Biol.* **33**, 1656–1668  
935 (2020).
- 936 52. Marçais, G. & Kingsford, C. A fast, lock-free approach for efficient parallel  
937 counting of occurrences of k-mers. *Bioinformatics* **27**, 764–770 (2011).
- 938 53. Xiao, C.-L. et al. MECAT: fast mapping, error correction, and de novo assembly  
939 for single-molecule sequencing reads. *Nat. Methods* **14**, 1072–1074 (2017).
- 940 54. Walker, B. J. et al. Pilon: an integrated tool for comprehensive microbial variant  
941 detection and genome assembly improvement. *PLoS One* **9**, e112963 (2014).
- 942 55. Prysycz, L. P., & Gabaldón, T. Redundans: an assembly pipeline for highly  
943 heterozygous genomes. *Nucleic Acids Res.* **44**, e113 (2016).
- 944 56. Zhang, Z., Schwartz, S., Wagner, L. & Miller, W. A greedy algorithm for aligning  
945 DNA sequences. *J. Comput. Biol.* **7**, 203–214 (2000).
- 946 57. English, A. C. et al. Mind the gap: upgrading genomes with Pacific Biosciences  
947 RS long-read sequencing technology. *PLoS ONE* **7**, e47768 (2012).
- 948 58. Sahlin, K., Chikhi, & Arvestad, R. L. Assembly scaffolding with PE-  
949 contaminated mate-pair libraries. *Bioinformatics* **32**, 1925–1932 (2016).
- 950 59. Belton, J. M. et al. Hi-C: a comprehensive technique to capture the conformation  
951 of genomes. *Methods* **58**, 268–276 (2012).
- 952 60. Servant, N. et al. (2015) HiC-Pro: an optimized and flexible pipeline for Hi-C  
953 data processing. *Genome Biol.* **16**, 259.
- 954 61. Durand, N.C. et al. Juicer provides a one-click system for analyzing loop-

- 955 resolution Hi-C experiments. *Cell Syst.* **3**, 95–98 (2016).
- 956 62. Dudchenko, O. et al. De novo assembly of the *Aedes aegypti* genome using Hi-C  
957 yields chromosome-length scaffolds. *Science* **356**, 92–95 (2017).
- 958 63. Simão, F. A., Waterhouse, R. M., Ioannidis, P., Kriventseva, E. V. & Zdobnov, E.  
959 M. BUSCO: assessing genome assembly and annotation completeness with  
960 single-copy orthologs. *Bioinformatics* **31**, 3210–3212 (2015).
- 961 64. Wu, T. D. & Watanabe, C. K. GMAP: a genomic mapping and alignment program  
962 for mRNA and EST sequences. *Bioinformatics* **21**, 1859–1875 (2005).
- 963 65. Benson, G. Tandem repeats finder: a program to analyze DNA sequences. *Nucleic  
964 Acids Res.* **27**, 573–580 (1999).
- 965 66. Bao, W., Kojima, K. K. & Kohany, O. Repbase Update, a database of repetitive  
966 elements in eukaryotic genomes. *Mobile DNA* **6**, 11 (2015).
- 967 67. Xu, Z. & Wang, H. LTR\_FINDER: an efficient tool for the prediction of full-  
968 length LTR retrotransposons. *Nucleic Acids Res.* **35**, W265–W268 (2007).
- 969 68. Edgar, R. C. & Myers, E. W. PILER: identification and classification of genomic  
970 repeats. *Bioinformatics* **21**, i152–i158 (2005).
- 971 69. Price, A. L., Jones, N. C. & Pevzner, P. A. De novo identification of repeat  
972 families in large genomes. *Bioinformatics* **21**, i351–i358 (2005).
- 973 70. Lowe, T. M. & Eddy, S. R. tRNAscan-SE: a program for improved detection of  
974 transfer RNA genes in genomic sequence. *Nucleic Acids Res.* **25**, 955–964  
975 (1997).
- 976 71. Nawrocki, E. P. & Eddy, S. R. Infernal 1.1: 100-fold faster RNA homology

- 977 searches. *Bioinformatics* **29**, 2933–2935 (2013).
- 978 72. Nawrocki, E.P. et al. Rfam 12.0: updates to the RNA families database. *Nucleic*  
979 *Acids Res.* **43**, D130–D137 (2015).
- 980 73. Holt, C. & Yandell, M. MAKER2: an annotation pipeline and genome-database  
981 management tool for second-generation genome projects. *BMC Bioinformatics*  
982 **12**, 491 (2011).
- 983 74. Kim, D., Langmead, B. & Salzberg, S.L. HISAT: a fast spliced aligner with low  
984 memory requirements. *Nat. Methods* **12**, 357–360 (2015).
- 985 75. Pertea, M. et al. StringTie enables improved reconstruction of a transcriptome  
986 from RNA-seq reads. *Nat. Biotechnol.* **33**, 290–295 (2015).
- 987 76. Johnson, A. D. et al. SNAP: a web-based tool for identification and annotation of  
988 proxy SNPs using HapMap. *Bioinformatics* **24**, 2938–2939 (2008).
- 989 77. Stanke, M. & Morgenstern, B. AUGUSTUS: a web server for gene prediction in  
990 eukaryotes that allows user-defined constraints. *Nucleic Acids Res.* **33**, W465–  
991 W467 (2005).
- 992 78. Buels, R. et al. JBrowse: a dynamic web platform for genome visualization and  
993 analysis. *Genome Biol.* **17**, 66 (2016).
- 994 79. Buchfink, B., Xie, C. & Huson, D.H. Fast and sensitive protein alignment using  
995 DIAMOND. *Nat. Methods* **12**, 59–60 (2015).
- 996 80. Bairoch, A. & Apweiler, R. The SWISS-PROT protein sequence database and its  
997 supplement TrEMBL in 2000. *Nucleic Acids Res.* **28**, 45–48 (2000).
- 998 81. Kanehisa, M., Sato, Y., Kawashima, M., Furumichi, M. & Tanabe, M. KEGG as a

- 999 reference resource for gene and protein annotation. *Nucleic Acids Res.* **44**, D457–  
1000 D462 (2016).
- 1001 82. Jones, P. et al. InterProScan 5: genome-scale protein function classification.  
1002 *Bioinformatics* **30**, 1236–1240 (2014).
- 1003 83. Conesa, A. et al. Blast2GO: a universal tool for annotation, visualization and  
1004 analysis in functional genomics research. *Bioinformatics* **21**, 3674–3676 (2005).
- 1005 84. Li, L., Stoeckert, C. J., Jr. & Roos, D. S. OrthoMCL: identification of ortholog  
1006 groups for eukaryotic genomes. *Genome Res.* **13**, 2178–2189 (2003).
- 1007 85. Li, H. et al. TreeFam: a curated database of phylogenetic trees of animal gene  
1008 families. *Nucleic Acids Res.* **34**, D572–D580 (2006).
- 1009 86. Edgar, R. C. MUSCLE: multiple sequence alignment with high accuracy and high  
1010 throughput. *Nucleic Acids Res.* **32**, 1792–1797 (2004).
- 1011 87. Capella-Gutierrez, S., Silla-Martinez, J.M. & Gabaldon, T. trimAl: a tool for  
1012 automated alignment trimming in large-scale phylogenetic analyses.  
1013 *Bioinformatics* **25**, 1972–1973 (2009).
- 1014 88. Guindon, S., Delsuc, F., Dufayard, J. F. & Gascuel, O. Gascuel, Estimating  
1015 maximum likelihood phylogenies with PhyML. *Methods Mol. Biol.* **537**, 113–137  
1016 (2009).
- 1017 89. Yang, Z. PAML 4: phylogenetic analysis by maximum likelihood. *Mol. Biol.*  
1018 *Evol.* **24**, 1586–1591 (2007).
- 1019 90. De Bie, T., Cristianini, N., Demuth, J. P. & Hahn, M. W. CAFE: a computational  
1020 tool for the study of gene family evolution. *Bioinformatics* **22**, 1269–1271 (2006).

- 1021 91. Tang, H. et al. Unraveling ancient hexaploidy through multiply-aligned  
1022 angiosperm gene maps. *Genome Res.* **18**, 1944–1954 (2008).
- 1023 92. Schwartz, S. et al. Human-mouse alignments with BLASTZ. *Genome Res.* **13**,  
1024 103–107 (2003).
- 1025 93. Bailey, J. A., Yavor, A. M., Massa, H. F., Trask, B. J. & Eichler, E. E. Segmental  
1026 duplications: organization and impact within the current human genome project  
1027 assembly. *Genome Res.* **11**, 1005–1017 (2001).
- 1028 94. Birney, E., Clamp, M. & Durbin, R. GeneWise and Genomewise. *Genome Res.*  
1029 **14**, 988–995 (2004).
- 1030 95. Ruan, J., Li, H., Chen, Z. & Coghlan, A. TreeFam: 2008 Update. *Nucleic Acids*  
1031 *Res.* **36**, D735–D740 (2008).
- 1032 96. Tholl, D. et al. Practical approaches to plant volatile analysis. *Plant J.* **45**, 540–  
1033 560 (2006).
- 1034 97. Wen, B., Mei, Z., Zeng, C. & Liu, S. metaX: a flexible and comprehensive  
1035 software for processing metabolomics data. *BMC Bioinformatics* **18**, 183 (2017).
- 1036 98. Wen, P. et al. The sex pheromone of a globally invasive honey bee predator, the  
1037 Asian eusocial hornet, *Vespa velutina*. *Sci. Rep.* **7**, 12956 (2017).
- 1038 99. Chen, Y., Chen, Y., Shi, C. & Huang, Z. et al. SOAPnuke: a MapReduce  
1039 acceleration-supported software for integrated quality control and preprocessing  
1040 of high-throughput sequencing data. *Gigascience* **7**, 1–6 (2018).
- 1041 100. Langmead, B. & Salzberg, S. L. Fast gapped-read alignment with Bowtie 2. *Nat.*  
1042 *Methods* **9**, 357–359 (2012).

- 1043 101.Li, B. & Dewey, C. N. RSEM: accurate transcript quantification from RNA-Seq  
1044 data with or without a reference genome. *BMC Bioinformatics* **12**, 323 (2011).
- 1045 102.Tian, X., Chen, L., Wang, J., Qiao, J. & Zhang, W. Quantitative proteomics  
1046 reveals dynamic responses of *Synechocystis* sp. PCC 6803 to next-generation  
1047 biofuel butanol. *J. Proteomics* **78**, 326–345 (2013).
- 1048 103.Wen, B., Zhou, R., Feng, Q., Wang, Q., Wang, J. & Liu, S. IQuant: an automated  
1049 pipeline for quantitative proteomics based upon isobaric tags. *Proteomics* **14**,  
1050 2280–2285 (2014).
- 1051 104.Brosch, M., Yu, L., Hubbard, T. & Choudhary, J. Accurate and sensitive peptide  
1052 identification with Mascot Percolator. *J. Proteome Res.* **8**, 3176–3181 (2009).
- 1053 105.Savitski, M. M., Wilhelm, M., Hahne, H., Kuster, B. & Bantscheff, M. A scalable  
1054 approach for protein false discovery rate estimation in large proteomic data sets.  
1055 *Mol. Cell. Proteomics* **14**, 2394–2404 (2015).
- 1056 106.Cox, J. & Mann, M. MaxQuant enables high peptide identification rates,  
1057 individualized p.p.b.-range mass accuracies and proteome-wide protein  
1058 quantification. *Nat. Biotechnol.* **26**, 1367–1372 (2008).
- 1059 107.Bruderer, R. et al. Extending the limits of quantitative proteome profiling with  
1060 data-independent acquisition and application to acetaminophen-treated three-  
1061 dimensional liver microtissues. *Mol. Cell. Proteomics* **14**, 1400–1410 (2015).
- 1062 108.Dunn, W.B. et al. Procedures for large-scale metabolic profiling of serum and  
1063 plasma using gas chromatography and liquid chromatography coupled to mass  
1064 spectrometry. *Nat. Protoc.* **6**, 1060–1083 (2011).

- 1065 109.Love, M. I., Huber, W. & Anders, S. Moderated estimation of fold change and  
1066 dispersion for RNA-seq data with DESeq2. *Genome Biol.* **15**, 550 (2014).
- 1067 110.Choi, M. et al. MSstats: an R package for statistical analysis of quantitative mass  
1068 spectrometry-based proteomic experiments. *Bioinformatics* **30**, 2524–2526  
1069 (2014).
- 1070 111.Wen, X.-L., Wen, P., Dahlsjö, C. A. L., Sillam-Dussès, D. & Šobotník, J.  
1071 Breaking the cipher: ant eavesdropping on the variational trail pheromone of its  
1072 termite prey. *Proc. R. Soc. B.* **284**, 20170121 (2017).
- 1073 112.Bailey, T. L. & Elkan, C. Fitting a mixture model by expectation maximization to  
1074 discover motifs in biopolymers. *Proc. Int. Conf. Intell. Syst. Mol. Biol.* **2**, 28–36  
1075 (1994).
- 1076 113.Langfelder, P. & Horvath, S. WGCNA: an R package for weighted correlation  
1077 network analysis. *BMC Bioinformatics* **9**, 559 (2008).
- 1078 114.Yip, A. M. & Horvath, S. Gene network interconnectedness and the generalized  
1079 topological overlap measure. *BMC Bioinformatics* **8**, 22 (2007).
- 1080 115.Langfelder, P., Zhang, B. & Horvath, S. Defining clusters from a hierarchical  
1081 cluster tree: the dynamic tree cut package for R. *Bioinformatics* **24**, 719–720  
1082 (2008).
- 1083 116.Lescot, M. et al. PlantCARE, a database of plant cis-acting regulatory elements  
1084 and a portal to tools for in silico analysis of promoter sequences. *Nucleic Acids*  
1085 *Res.* **30**, 325–327 (2002).
- 1086 117.Gendrel, A.V., Lippman, Z., Martienssen, R. & Colot V. Profiling histone

1087 modification patterns in plants using genomic tiling microarrays. *Nat. Methods* **2**,  
1088 213–218 (2005).

1089 **Table 1 | Summary statistics for the assembly of *F. pumila var. pumila* and *W.***  
 1090 ***pumilae* genomes.**

1091

Chromosome ID	<i>F. pumila var. pumila</i>		<i>W. pumilae</i>	
	No. of genes	Length (bp)	No. of genes	Length (bp)
Chr1	1,697	20,463,500	816	21,315,831
Chr2	1,871	21,202,951	2,076	59,985,216
Chr3	2,335	23,199,346	2,631	66,440,284
Chr4	2,412	23,721,380	2,225	54,409,331
Chr5	3,327	31,603,922	2,281	59,419,729
Chr6	1,649	20,816,579	2,263	55,968,755
Chr7	2,070	23,331,000		
Chr8	2,097	21,006,959		
Chr9	1,856	21,788,500		
Chr10	1,740	20,107,953		
Chr11	1,798	22,360,920		
Chr12	2,000	20,847,995		
Chr13	2,526	34,592,857		
Number of contigs	543		102	
Total length of contigs (Mb)	315.7		318.2	
Contig N50 (Mb)	2.3		10.9	
Anchored genome content (Mb)	304.8		317.5	
Anchored rate	96.6%		99.8%	
Scaffold N50 (Mb)	22.4		59.4	
Number of genes	28,187		12,316	

1092

1093 **Figure legends**

1094 **Fig. 1 | Fig-pollinator mutualism between *F. pumila* var. *pumila* and *Wiebesia***  
1095 ***pumilae* and determination of the compound attracting *W. pumilae*.** **a**, Life cycle  
1096 of *W. pumilae* based on four fig developmental stages (pre-receptive, receptive, post-  
1097 receptive and mature stages). This *Ficus* species is dioecious with figs on female trees  
1098 growing long-styled female florets (seed florets) that are not available for pollinator  
1099 oviposition. Therefore, female trees only produce seeds, while figs on functional male  
1100 trees contain both male florets and short-styled female florets (feeder florets) that can  
1101 be used by female pollinators for oviposition to support the larvae of the pollinators.  
1102 At the receptive stage, adult female pollinators are attracted by host-specific VOCs  
1103 and enter figs only through ostiole (lined with bracts), either ovipositing into ovules of  
1104 feeder florets in functional male figs or pollinating seed florets inside female figs.  
1105 Pollinator larvae develop in induced galled ovules and both larvae and seeds grow  
1106 during the post-receptive stage. At the mature stage, after mating with adult males,  
1107 adult female pollinators leave their natal figs carrying pollen donated by mature male  
1108 florets and search for receptive figs and complete the cycle. **b**, Electrophysiological  
1109 responses of adult females of *W. pumilae* to the VOCs extracted from *F. pumila* var.  
1110 *pumila* figs at receptive stage using GC–EAD. Each curve represents the response of a  
1111 single female pollinator. **c**, Electrophysiological responses of adult female pollinators  
1112 to the synthesized standard of each tentative VOC compound (each  
1113 electroantennogram curve represents five overlapped replicates). **d**, Preference of  
1114 adult female pollinators to different tentative compounds using Y-tube olfactometer

1115 tests (Supplementary Table 9).

1116

1117 **Fig. 2 | Molecular mechanisms of the specific host identification of *W. pumilae*. a,**

1118 Numbers of genes in the four olfactory-related gene families (odorant-binding

1119 proteins (OBPs), olfactory receptors (ORs), chemosensory proteins (CSPs) and

1120 ionotropic receptor (IRs)) in different insect species. Significantly contracted families

1121 (\*\*\*:  $p < 0.001$ ) were shown for *W. pumilae* and *C. solmsi*, and species were ranked

1122 according to their phylogeny (Supplementary Fig. 4b). **b,** Transcription and

1123 translation of OBP genes of adult females of *W. pumilae* not contacting (as the

1124 control) and contacting the VOCs emitted by *F. pumila* var. *pumila* figs at the

1125 receptive stage (Supplementary Table 10). **c,** Motif analysis predicting the most likely

1126 *W. pumilae* OBPs that can bind to decanal and nonanal (Supplementary Fig. 9). **d,** The

1127 binding affinities ( $K_D$ ) of the predicted OBPs to decanal and nonanal using surface

1128 plasmon resonance (SPR) experiments (Supplementary Fig. 10 and Supplementary

1129 Table 11). Lower  $K_D$  indicates higher binding affinity, and error bars represent

1130 standard errors calculated by parameter estimation in steady state affinity model.

1131

1132 **Fig. 3 | Regulation of gene expression in attractant biosynthesis in figs of *F.***

1133 *pumila* var. *pumila*. **a,** Pathways associated with biosynthesis of decanal and nonanal

1134 (fatty acid biosynthesis (ko00061), elongation (ko00062) and metabolism (ko00071

1135 and ko00592)). **b,** Fold changes of all PSDs and their transcriptomic expression

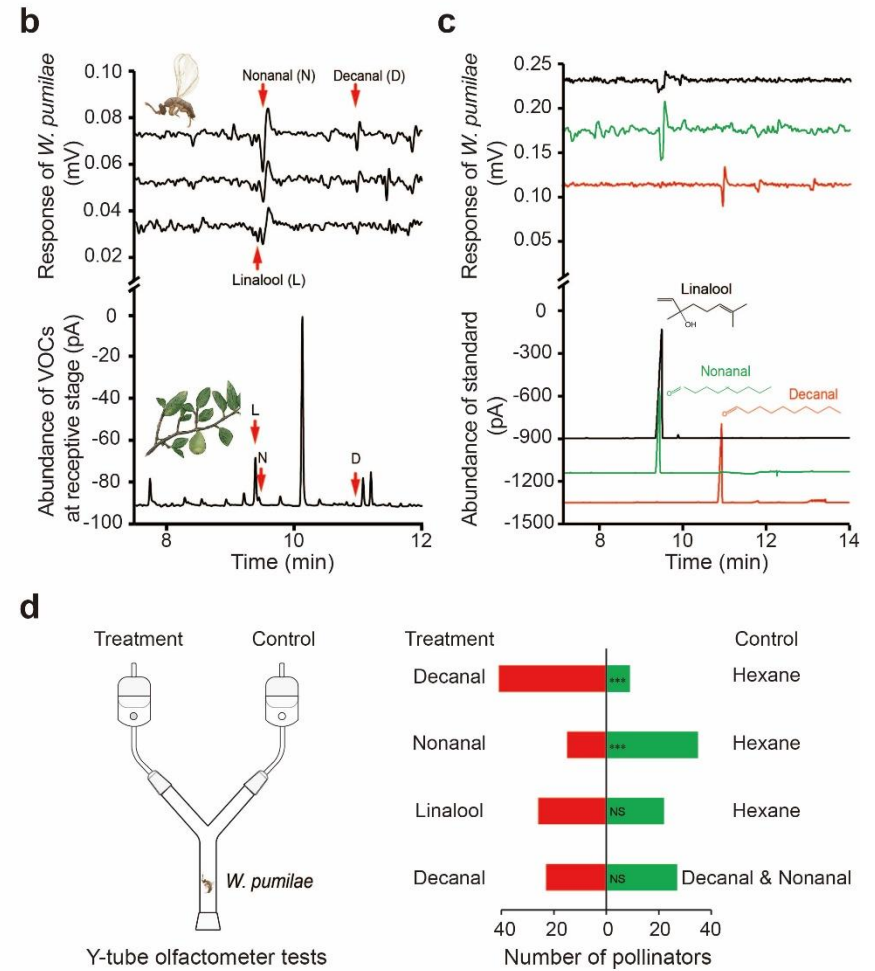
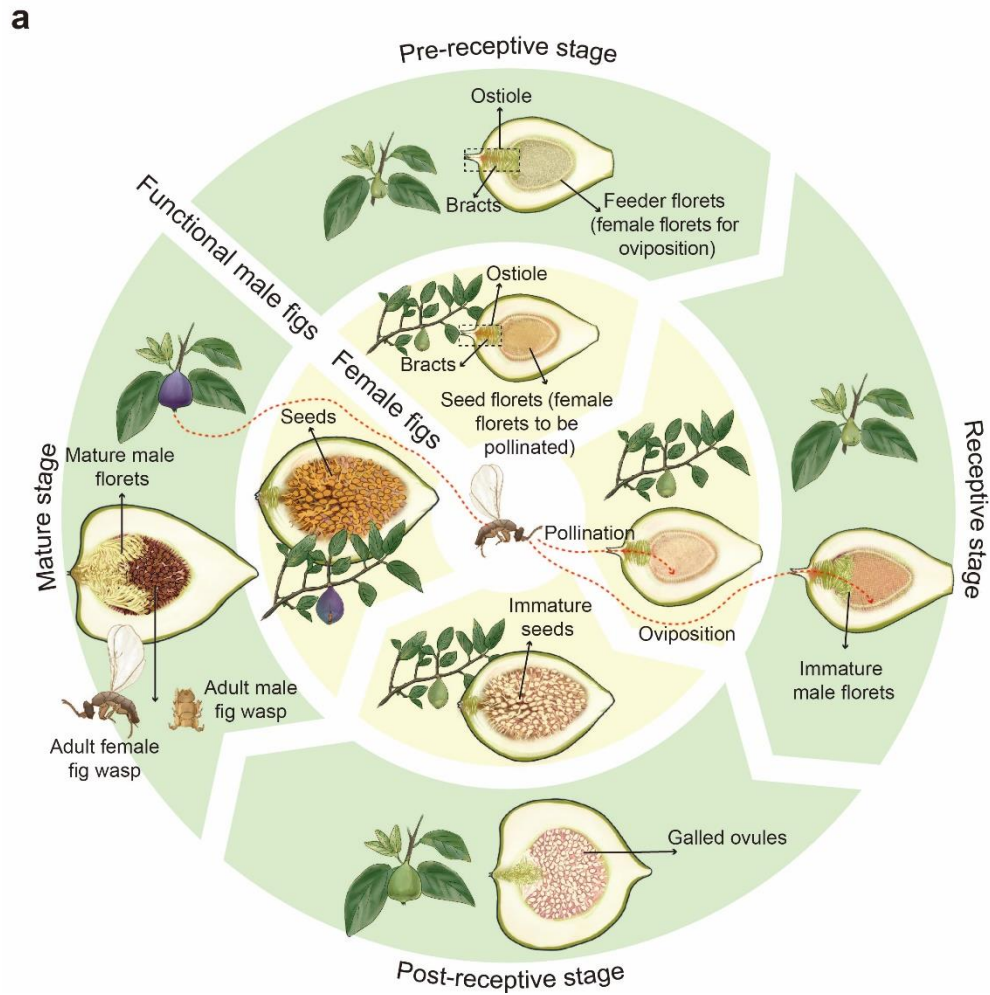
1136 between receptive and pre-receptive stages in ostiolar types in proteomes

1137 (Supplementary Table 12). <sup>NS</sup>: p>0.05, \* : p<0.05, \*\* : p<0.01, \*\*\* : p<0.001. **c-e**, Results  
1138 of *in vitro* functional characterization of the four key genes in the biosynthesis of  
1139 decanal and nonanal. The peaks of synthesized standards and reaction products  
1140 (treatments with enzyme added for three replicates) were shown for each key gene.  
1141 Because there are two steps in the catalytic reaction of the two ACSLs, we showed the  
1142 ion intensity of both the intermediate product (hexadecanoyl-AMP) and the final  
1143 product (hexadecanoyl-CoA) separated by LC-MS. The reaction products of the  
1144 ALDH and the ADH (decanal and decanol) were identified using GC-MS. **f**,  
1145 Transcriptomic expression of genes in the co-expression module including two key  
1146 genes and the transcription factors predicted to regulate the expression of these two  
1147 key genes (Supplementary Tables 13 and 14). **g-h**, Results of ChIP-qPCRs (% input  
1148 and fold enrichment) showing the evidence that the predicted transcription factors can  
1149 bind to the promoter regions of *FpumACSL10* (FPUM\_023966-RA) and  
1150 *FpumALDH1* (see Supplementary Tables 12 and 13). Error bars represent standard  
1151 errors of experimental results.

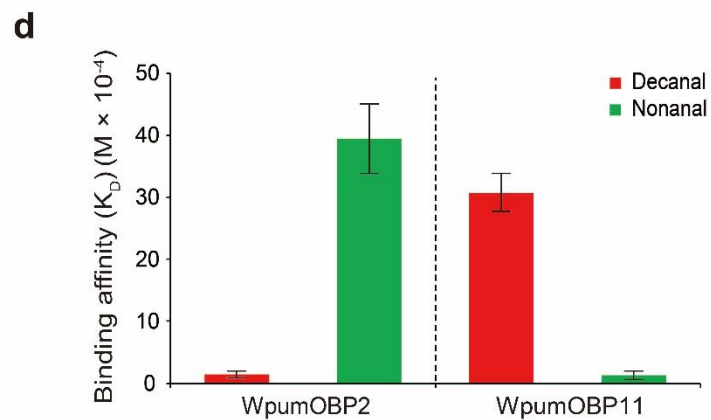
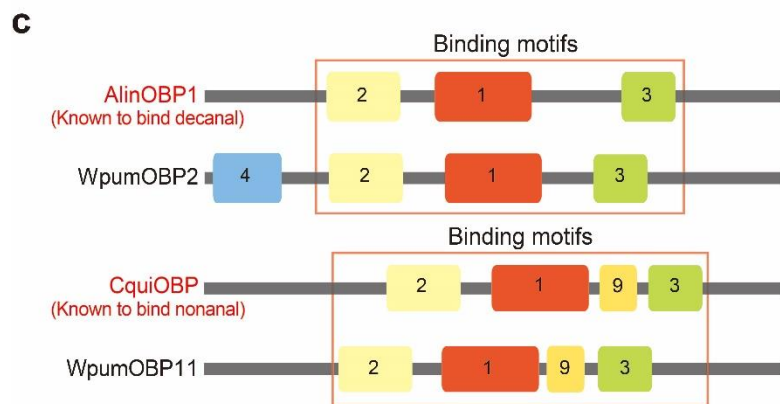
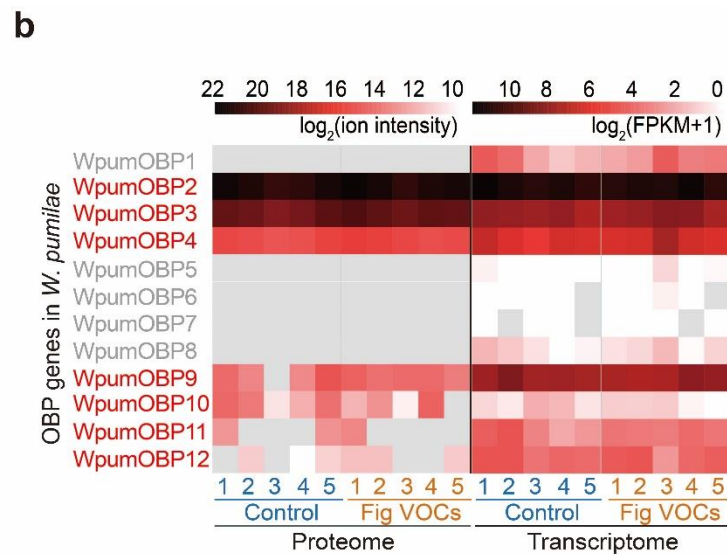
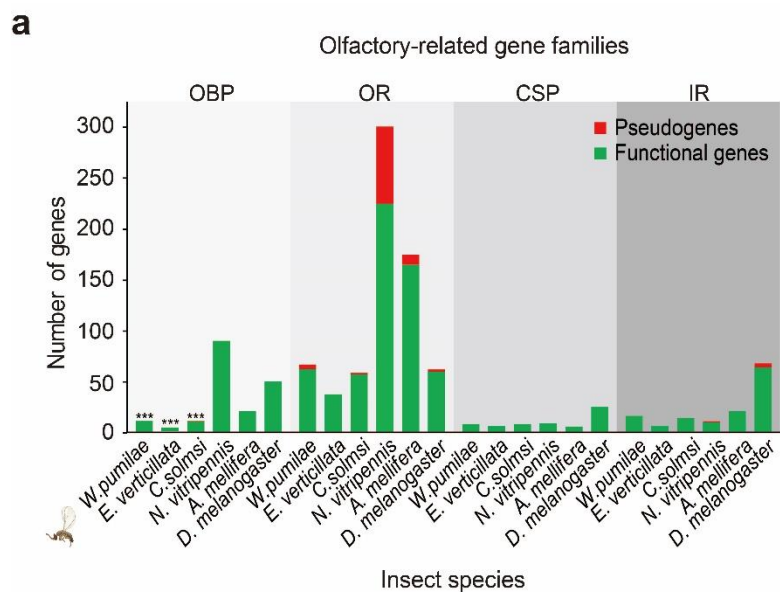
1152

1153 **Fig. 4 | Metabolic and genomic signature of antagonistic interaction between *F.***  
1154 ***pumila var. pumila* and *W. pumilae*.** **a**, Results of PLS-DA for terpenoids (triterpenes  
1155 and sesquiterpenes) and phenylpropanoids. Each oval indicates the 95% confidence  
1156 intervals of a sample group. **b**, Distribution of SMCDs across fates of female florets.  
1157 No SMSDs between feeder and seed florets and only three SMSDs (two  
1158 downregulated and one upregulated) between galled ovules and seeds were found in

1159 the pathways related to plant chemical defenses (Supplementary Fig. 12). **c**, Largely  
1160 matched turnover of SMSDs in feeder floret-galled ovule and seed floret-seed  
1161 transitions (using Spearman's rank correlation tests). **d**, Numbers of genes in  
1162 CYP450, CCE and GST gene families in different insect species. Significantly  
1163 contracted families (\*\*\*:  $p < 0.001$ ) were shown for *W. pumilae* and *C. solmsi*.

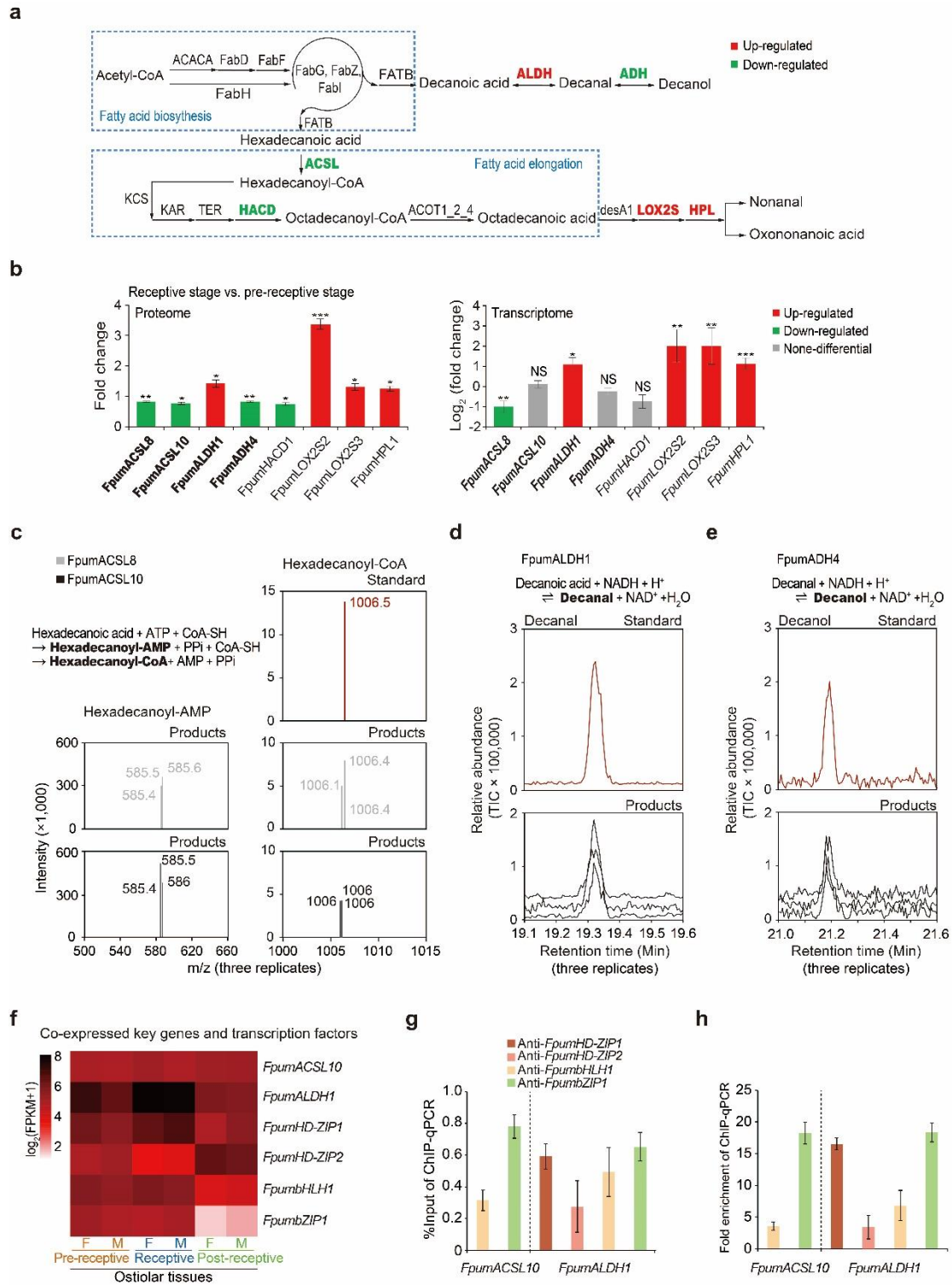


1164  
1165 Fig. 1.  
1166



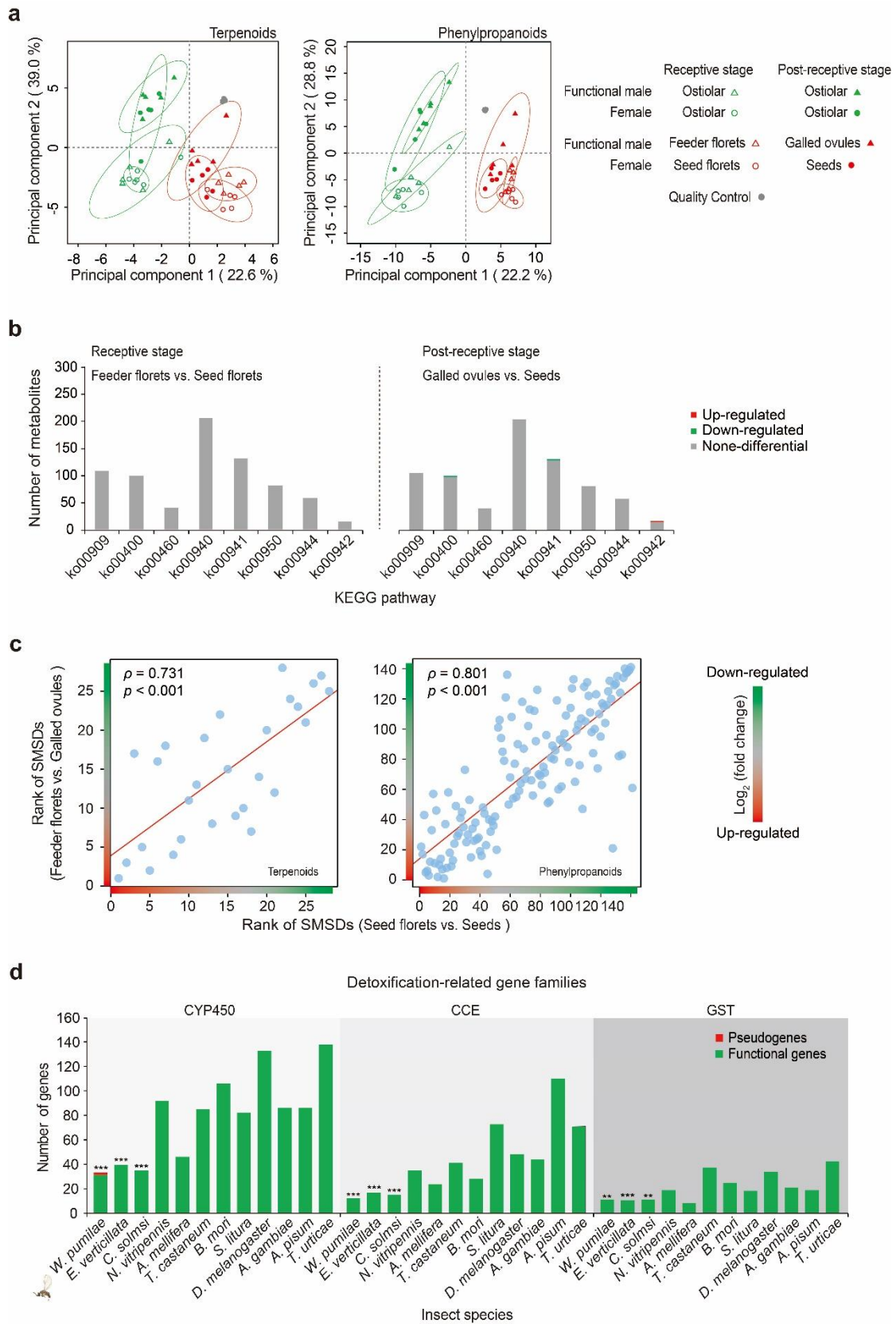
1167

1168 Fig. 2.



1169

1170 Fig. 3



1171  
1172

Fig. 4